IEEE TRANSACTIONS ON ROBOTICS, Volume 35, Issue 3, 2019, pp. 653-668
DOI: 10.1109/TRO.2019.2896436

Trajectory Optimisation for Target Localisation with Bearing-Only Measurement

Shaoming He, Hyo-Sang Shin*, Antonios Tsourdos

***Abstract*—This paper considers the problem of two-dimensional (2D) constrained trajectory optimisation of a point-mass aerial robot for constant-manoeuvring target localisation using bearing-only measurement. A performance metric that can be utilised in trajectory optimisation to maximise target observability is proposed first based on geometric conditions. One-step optimal manoeuvre that maximises the observability criterion is then derived analytically for moving targets. The heading angle constraint is also incorporated in the proposed optimal manoeuvre derivation to support practical application. Numerical simulations with some comparisons are presented to validate the analytical findings.**

***Index Terms*—Target localisation, Bearing-only measurement, Trajectory optimisation, Physical constraint**

I. Introduction

Small-scale robots, especially in aerial robotics, have been widely used and show great potentials in both civilian and military applications. The issue is that the operations of these small-scale aerial robots are constrained by limited payload, power and endurance. This has led to proliferation of numerous lightweight, low-cost and energy efficient onboard sensors. A particularly interesting mission for small robots is to localise and track targets of interest [1]–[6]. However, since most low-cost and lightweight sensors are passive sensors, e.g., optical or infrared camera, the utilisation of these sensors in target localisation usually suffers from the observability problem. Therefore, system observability becomes a fundamental requirement for bearing-only target localisation [7].

When employing passive sensors for target localisation, only the bearing or line-of-sight (LOS) angle can be measured. It is well known that the bearing angle measurement cannot provide relative range information without any relative manoeuvre, that is, the relative states between the observer and the target are unobservable under certain conditions. Fundamentally, only when the target is observable, the observer can localise or track the target. To this end, observability conditions for bearing-only target localisation are widely studied over past years. In [7], [8], the authors derived closed-form observability criteria for 2D constant moving target localisation. The results revealed that the observer acceleration should satisfy a certain condition to guarantee a certain degree of observability, which seem to be the pioneer works in this domain. As an extension of [7], the authors in [9] derived the observability condition for constant accelerating target localisation. The work in [10] further generalised the condition to Nth order target dynamics and further revealed that the observability condition derived in [7] is only necessary but not sufficient. In [11], [12], the authors proposed a general observability condition for angle-only navigation to determine the relative orbital motion and provided the conditions where the unobservable manoeuvres occur. By using a pseudo-linear structure of the pseudo-measurements, necessary and sufficient conditions, that can be applied to general target motions, for observability analysis were proposed in [13]. With a few assumptions, a closed-form metric that could be utilised to quantify system observability for manoeuvring target was derived in [14]. This analytical criterion essentially coincides with previously suggested metric given in [15] for constant moving targets.

Since system observability depends on the relative geometry [16]–[19], the trajectory of the observer poses a direct impact on the achievable estimation performance [20]–[23]. For this reason, it is known that trajectory optimisation, maximising system observability, can yield significant benefits for target tracking with bearing-only measurement to improve the quality of perceptual results [24]. Optimal observer trajectory that maximises system observability is generated in [3], [21], [25]–[27] by maximising the determinant of Fisher information matrix (FIM) over a finite time horizon. The rationale of using FIM for a cost function, also known as objective function, lies in that the inverse of FIM prescribes a lower bound of the estimation error covariance of an unbiased filter [28]. To minimise the sensing time and ensure bounded estimation uncertainty, an approximate algorithm to plan the bearing data gathering path was proposed in [29], where the determinant of FIM was utilised to quantify the estimation performance. Different from [25], [26], the determinant of error covariance matrix was employed as the cost function in [30], [31] for trajectotry optimisation. Using the same objective function, exhaustive search was utilised in [32] to find optimal sensor heading commands with motion constraints. On the basis of the nonlinear observability analysis tool, i.e., Observability Gramian (OG) [33], the authors in [34], [35] provided online gradient descent path planning strategies to actively maximise the smallest eigenvalue of the OG. A cautious greedy active sensing strategy was proposed in [36], [37] for localising a stationary target with bearing-only measurement in minimum time. Incorporating communication range and no-fly zone constraints into account, a numerical trajectory planning for target localisation with bearing-only measurement using multiple robots was proposed in [38]. An algorithm for cooperative active localisation of stationary targets using mobile bearing sensors was suggested in [39] by leveraging the largest

Shaoming He, Hyo-Sang Shin and Antonios Tsourdos are with the School of Aerospace, Transport and Manufacturing, Cranfield University, Cranfield MK43 0AL, UK (email: {shaoming.he,h.shin,a.tsourdos}@cranfield.ac.uk)
*Corresponding author.

eigenvalue of FIM as the cost function. To improve bearing-only observability while simultaneously consider other mission objectives, multi-objective trajectory optimisation problem was formulated and solved in [21], [40], [41]. Unfortunately, this particular problem formulated is not amendable to simple analytical solution. Hence, these approaches use numerical methods to find optimal solutions and consequently require high onboard computational power. As the onboard computational power is limited in low-cost and lightweight robots, those approaches are not suitable for such robots. Moreover, optimisation over a finite time horizon requires accurate target dynamics, which becomes prohibitive in practice, especially for hostile targets. These issues can be alleviated by applying one-step analytical optimisation as in [42]: optimal trajectory was obtained for ground robots by minimising the trace of the estimation error covariance matrix in one step in the work. However, since physical constraints of the robot are not rigorously considered, the solution derived in [42] might become infeasible for the robot.

This paper aims to develop an analytically optimal trajectory optimisation algorithm in consideration of physical constraints for constant-manoeuvring target localisation with bearing-only measurement. The contributions of this paper are twofold:

(1) Unlike previous approaches using FIM or error covariance matrix, this paper finds a performance measure of observability based on geometric conditions and utilises it as a pertinent cost function. While it is known that the relative geometry conditions determine the observability, there has been no attempt to obtain a geometry-based estimation performance measure for bearing-only-based target localisation available in the literature. Determining the performance measure, we provide a geometric interpretation on how the relative geometry influences the system observability. Such interpretation enables more intuitive and perhaps better insights to the relationship between the geometric condition and observability.

(2) This paper derives a closed-form solution that maximises the geometric observability measure formulated and meets physical constraints such as minimum turning rate. The resultant analytical solution, given as heading angle input command, is simple to be implemented in practice. Up to the best of our knowledge, no closed-form solution with a physical constraint is available in existing literature.

Realistic scenarios are simulated to illustrate and evaluate the performance of the proposed algorithm, and the results are compared with those of the existing analytical approach proposed in [42] and the approach in [14]. The simulation results reveal that the proposed algorithm meets the considered physical constraint unlike the approach from [42]. They also show that optimising the proposed geometric performance metric generates higher system observability than optimising the analytical measure derived in [14], thus leading to improved estimation performance.

The rest of the paper is organised as follows. Section II presents some preliminaries and backgrounds. Section III derives a geometric metric for observability analysis, followed by the optimal manoeuvre derivation shown in Sec. IV. Then, some simulations and conclusions are offered.

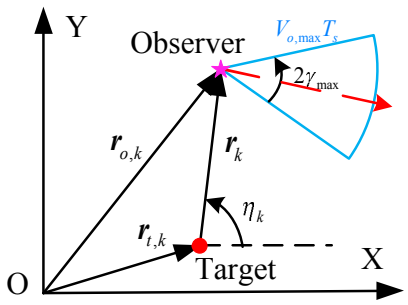

Fig. 1. Geometric relationship between the observer and the target at time step k in an inertial coordinate. The observer is represented by a magenta pentagram and the red circle denotes the target. The red vector stands for the observer heading direction at previous time step. The maximum permissible move region of the observer at current time instant is given by the blue sector with radius $V_{o,\max}T_s$ and angle $2\gamma_{\max}$.

II. Backgrounds and Preliminaries

This section provides some necessary preliminaries of vehicle kinematics model and bearing-only measurement model to facilitate the analysis in the following sections.

A. Vehicle Kinematics

This work assumes that the observer is equipped with a high-performance low-level flight control system that provides velocity tracking, heading and altitude hold functions. This study aims to design guidance input to this low-level controller for target localisation and only concerns the 2D motions. The rationale of leveraging simple 2D engagement is that typical aerial robots provide roll stabilisation and therefore the 3D guidance problem can be decoupled into horizontal and vertical channels using the well-known separation concept. The vehicle's kinematics in a 2D environment is given by

$$\begin{aligned} \dot{x}_o &= V_o \cos\gamma_o \\ \dot{y}_o &= V_o \sin\gamma_o \end{aligned} \tag{1}$$

where (x_o, y_o) stands for the observer's position in an inertial coordinate. γ_o is the observer's heading angle and $V_o \in (0, V_{o,\max}]$ denotes the observer's velocity with $V_{o,\max}$ being the maximum permissible velocity. Note that the observer's velocity V_o is assumed to be larger than the target's velocity in this paper.

In practice, the observer heading change between two consecutive time steps is constrained due to physical turning rate limitation as

$$|\gamma_{o,k} - \gamma_{o,k-1}| \leq \gamma_{\max} \triangleq \omega_{\max} T_s \tag{2}$$

where $\gamma_{o,k}$ represents the heading angle at time step k, $\omega_{\max}$ the maximum permissible turning rate of the observer, and T_s the sampling time.

B. Measurement Model

Figure 1 shows the geometric relationship between the observer and the target at time step k. $X-O-Y$ stands for the inertial coordinate. The notations $\mathbf{r}_{o,k} = [x_{o,k}, y_{o,k}]^T$ and $\mathbf{r}_{t,k} = [x_{t,k}, y_{t,k}]^T$ represent the position vectors of the observer and the target at time step k, respectively.

$\mathbf{r}_k = \mathbf{r}_{o,k} - \mathbf{r}_{t,k}$ denotes the relative position vector between the observer and the target. With heading constraint (2), the maximum region the observer can travel at current time step is described by a sector, as shown in Fig. 1. At time step k, the observer only has access to its bearing angle measurement η_k toward the target. Therefore, the sensor measurement z_k is given by

$$z_k = \eta_k + \varepsilon \tag{3}$$

where ε denotes the sensor measurement noise.

Let $\mathbf{r}_k = [x_k, y_k]^T$, then, the sensor measurement z_k can also be formulated as

$$z_k = \arctan\left(\frac{y_k}{x_k}\right) + \varepsilon \tag{4}$$

From Eq. (4), it is clear that the relative distance is not directly measurable by bearing angle η_k, that is, (x_k, y_k) and $(\mu x_k, \mu y_k)$ with $\mu \in \mathbb{R}^+$ provide the same bearing angle η_k. Therefore, certain manoeuvres have to be performed to make the range observable in a certain degree.

Remark 1. Note that the bearing angle in Eq. (4) is the direction of $\mathbf{r}_k$ with respect to a world/inertial frame. In practice, however, observers with onboard sensors, i.e., cameras, can only provide the direction of $\mathbf{r}_k$ with respect to the body frame. Therefore, additional observer attitude information from IMU is required to obtain η_k. For simplicity, we assume that the IMU provides accurate attitude information by a well-tuned filter and therefore only sensor noise is considered in measurement model (4). Note that this assumption has been widely used in active target localisation with bearing-only measurement [14], [39], [42], [43]. Although the IMU output has inevitable noise, it can be accumulated in ε and therefore the algorithm developed is still valid.

III. Geometric Analysis and Problem Formulation

This section first derives a geometric metric that can be utilised in trajectory optimisation to maximise system observability. Then, the problem formulation of the paper is stated.

A. Geometric Metric for Observability Maximisation

Change in the vehicle's velocity and its direction over a short interval, like over T_s, is usually negligible. Hence, for simplicity, it is assumed that both the observer and the target are piece-wise non-manoeuvring, i.e., moving with constant speed and constant direction between two consecutive time instants. Figure 2 shows the geometric relationship between the observer and the target in two consecutive time instants, where Fig. 2 (a) shows the geometric relationship in an inertial frame and Fig. 2 (b) provides the geometric relationship in a relative frame. Notice that the relative frame can accommodate moving target since the relative position vector $\mathbf{r}_k$ directly contains the information on target movement. In Fig. 2, $\delta\mathbf{r}_k$ represents the relative manoeuvre at time step k. σ is the separation angle between two consecutive relative position vectors.

Between two consecutive time instants, it is clear from Fig. 2 that the relative position vector $\mathbf{r}_{k+1}$ at next time step can be uniquely determined by triangulation if $\sigma \neq 0$ and $\mathbf{r}_k$ is available to the observer. Based on this observation, we assume that the relative position vector $\mathbf{r}_k$ is known for finding the optimal observer manoeuvre vector at time instant k in one-step trajectory optimisation. The validity of this assumption will be proved through a detailed observability analysis shown in Sec. IV E. Note that, if $\sigma = 0$, $\mathbf{r}_{k+1} = k_1\mathbf{r}_k$, $k_1 \in \mathbb{R}^+$. Then, it is impossible to distinguish the next step relative position vector from the current step relative position vector regardless of the angle measurement. Hence, the relative manoeuvre should satisfy the condition $\sigma \neq 0$, which coincides with the necessary observability condition that the LOS rate $\dot{\eta} = \sigma/T_s$ cannot be zero, derived in [9] for a non-manoeuvring target. Therefore, under the assumption that $\mathbf{r}_k$ is available, the robot can localise the target only when the robot-target relative geometry satisfies the condition $\sigma \neq 0$.

Let $\delta\rho \triangleq CE$ be the relative position estimation error at time step $k+1$ caused by the sensor bearing measurement error ε. Based on the law of sines, we have

$$\triangle OCE\text{: } \frac{\delta\rho}{\sin\varepsilon} = \frac{OE}{\sin\left[\pi - (\sigma + \varepsilon/2)\right]} = \frac{OE}{\sin\left(\sigma + \varepsilon/2\right)} \tag{5}$$

$$\triangle ODE\text{: } \frac{\|\delta\mathbf{r}_k\|}{\sin\left(\sigma - \varepsilon/2\right)} = \frac{OE}{\sin\alpha} \tag{6}$$

$$\triangle OAB\text{: } \frac{\|\mathbf{r}_{k+1}\|}{\sin\alpha} = \frac{\|\delta\mathbf{r}_k\|}{\sin\sigma} \tag{7}$$

Combining Eqs. (5) and (6), one can imply that

$$\delta\rho = \|\delta\mathbf{r}_k\| \left(\frac{\sin\alpha\sin\varepsilon}{\sin^2\sigma - \sin^2\left(\varepsilon/2\right)}\right) \tag{8}$$

where the fact that $\sin\left(a+b\right)\sin\left(a-b\right) = \sin^2 a - \sin^2 b$ is utilised in the derivation.

Assume that the sensor bearing measurement error ε is small, Eq. (8) can be reduced to

$$\delta\rho = \varepsilon\,\|\delta\mathbf{r}_k\| \left(\frac{\sin\alpha}{\sin^2\sigma}\right) \tag{9}$$

Substituting Eq. (7) into Eq. (9) yields the error square as

$$\delta\rho^2 = \varepsilon^2 \left(\frac{\|\mathbf{r}_{k+1}\|}{\sin\sigma}\right)^2 \tag{10}$$

The preceding equation reveals that the relative position estimation (or target localisation) error at next time step is characterised by the sensor measurement error ε, the separation angle σ and the relative range $\|\mathbf{r}_{k+1}\|$. This provides us better insights to the influence of relative geometric configuration on system observability.

Remark 2. Notice that Eq. (10) closely resembles the expression of geometric dilution of precision (GDOP), which is commonly leveraged in satellite navigation and geomatics engineering: the term $\left(\|\mathbf{r}_{k+1}\|/\sin\sigma\right)^2$ determines the sensitivity of estimation performance to bearing measurement errors.

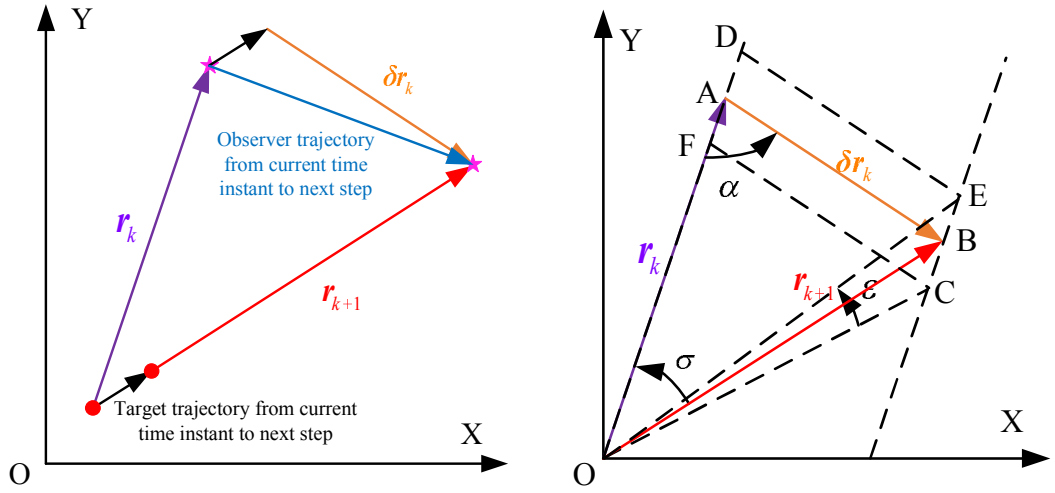

Fig. 2. Geometric relationship between the observer and the target in two consecutive time instants. (a) Geometric relationship in an inertial frame. The black line represents the target movement trajectory and the blue line stands for the observer movement trajectory at current time instant. The orange line refers to the relative movement trajectory. (b) Geometric relationship in a relative frame. The relative frame in (b) is defined by using the relative motion kinematics, e.g., relative range $\mathbf{r}_k$, and attaching the origin at the target position at time instant k. In (b), line $\overline{CE}$ is parallel to line $\overline{FD}$. Both lines $\overline{DE}$ and $\overline{FC}$ are parallel to line $\overline{AB}$ in (b).

B. Problem Formulation

The aim of the trajectory optimisation is to determine optimal manoeuvres that minimise target localisation error and also respect the physical constraints given in (2). To accomplish the aim, this paper formulates a discrete-time trajectory optimisation problem which is denoted as CTO_1.

CTO_1: find the observer manoeuvre at time step k, $\mathbf{v}_{o,k}$, which maximises the following objective function J

$$J = \left(\frac{\sin \sigma}{\|\mathbf{r}_{k+1}\|} \right)^2 \tag{11}$$

subject to

$$\begin{aligned} &|\gamma_{o,k} - \gamma_{o,k-1}| \leq \omega_{\max} T_s \\ &0 < V_{o,k} \leq V_{o,\max} \end{aligned} \tag{12}$$

Note that the observer manoeuvre at time step k is given as

$$\mathbf{v}_{o,k} = [V_{o,k} T_s \cos \gamma_{o,k}, V_{o,k} T_s \sin \gamma_{o,k}]^T \tag{13}$$

The cost function J is determined in consideration of $\delta\rho^2$ obtained in (10): since ε is determined by the sensing device, a practical way to reduce the estimation error is to find an optimal one-step observer manoeuvre that maximises the cost function J given by (11).

Remark 3. Geometrically, the minimisation of $\|\mathbf{r}_{k+1}\|$ and the maximisation of $|\sin \sigma|$ are two conflict objectives. Therefore, the information maximising manoeuvre obtained from $\max J$ will provide a proper balance between forcing σ to approach $\pm\pi/2$ and reducing the relative range. This means that the resulting optimal solution satisfies $-\pi/2 < \sigma < \pi/2$.

Remark 4. Note that, since Eq. (11) is provided in a closed form, it permits simple weighed inclusion inside a global trajectory optimisation problem as an auxiliary objective, allowing for an optimal solver to find manoeuvres that are beneficial in terms of observability enhancement while considering other objectives.

Remark 5. Assume that the range variation between two successive instants is negligible, i.e., $\|\mathbf{r}_k\| \approx \|\mathbf{r}_{k+1}\|$ and the separation angle is small, i.e., $\sin(\sigma) \approx \sigma$, the authors in [14] revealed that the determinant of the incremental of FIM at time step k is lower bounded by

$$|\Delta F_k| = |F_{k+1} - F_k| \geq c \left(\frac{\sigma}{\|\mathbf{r}_k\|} \right)^2 \tag{14}$$

where c is a constant depending on the measurement noise statistics and the time step. The notation F_k denotes the FIM at time instant k. It follows from Eq. (14) that maximising $(\sigma/\|\mathbf{r}_k\|)^2$ can increase the lower bound of $|\Delta F_k|$, leading to the increase of observability between two consecutive time steps. Therefore, $\hat{J} = (\sigma/\|\mathbf{r}_k\|)^2$ was utilised as the cost function in [14] to find optimal observer trajectory for information maximisation.

One can note that both J and $\hat{J}$ share a similar characteristic that target observability can be enhanced by increasing the absolute value of the separation angle σ. Apart from this similar property, the difference between cost functions J and $\hat{J}$ is clear: $\hat{J}$ ignores the variation of $\|\mathbf{r}_k\|$ while the proposed geometric measure relaxed this assumption. Conceptually, one can geometrically conclude from Fig. 2 (b) that smaller $\|\mathbf{r}_k\|$ provides lower estimation error with same bearing noise ε. With this in mind, it is expected that maximising J can generate improved estimation performance, compared to maximising $\hat{J}$. It is worthy to point out that the proposed cost function J gradually converges to $\hat{J}$ when $T_s \to 0$.

Remark 6. Different from [14], the authors in [42] provided a solution of trajectory optimisation by exploiting the trace of error covariance as a cost function, which directly characterises the average estimation variance. However, the turning

rate limit constraint was not considered in the optimisation, which means that the solution obtained in [42] might become infeasible in practice.

Remark 7. It should be pointed out that both [14] and [42] formulated their cost functions directly from classical estimation theory. However, the proposed cost function J is derived using simple geometric condition with clear physical meanings. This obviously reveals that how the observer-target relative geometry influences the estimation accuracy.

IV. Derivation of Optimal Manoeuvre for Target Localisation

This section will propose an analytical optimal manoeuvre that maximises the cost function J for target localisation with bearing-only measurement. We first derive the optimal solution without heading constraint and then extend to the case that the robot has limited turning rate to change its heading angle. Finally, target observability under the proposed approach will be analysed.

A. Optimal Manoeuvre without Heading Constraints

Excluding the heading constraint, *CTO*$_1$ reduces to *CTO*$_2$. *CTO*$_2$: find the observer manoeuvre at time step k, $\mathbf{v}_{o,k}$, which maximises the following objective function J

$$J = \left(\frac{\sin\sigma}{\|\mathbf{r}_{k+1}\|} \right)^2 \tag{15}$$

subject to

$$0 < V_{o,k} \leq V_{o,\max} \tag{16}$$

Let $\mathbf{v}_{t,k} = [v_{tx,k}, v_{ty,k}]^T \triangleq [V_{t,k}T_s\cos\gamma_{t,k}, V_{t,k}T_s\sin\gamma_{t,k}]^T$ be the target manoeuvre vector at time step k. Since the target velocity vector at current time step can be obtained from Kalman filter, $\mathbf{v}_{t,k}$ is known in trajectory optimisation. Figure 3 (a) shows the geometric relationship between the observer and the target within two consecutive time steps. Since $\mathbf{v}_{t,k}$ is fixed, $\bar{\mathbf{r}}_k$ is known in trajectory optimisation. The analytical solution of *CTO*$_2$ can be obtained using Lemmas 1 through 3.

Lemma 1. *Given the observer velocity $V_{o,k}$, the candidate optimal heading angle at time step k without any constraint is given by*

$$\gamma_{o,k}^{*,1} = \arcsin\left(-\frac{2V_{o,k}T_s\mathbf{r}_k^T\cdot\bar{\mathbf{r}}_k}{\sqrt{a^2+b^2}} \right) - \vartheta \tag{17}$$

$$\gamma_{o,k}^{*,2} = \pi - \arcsin\left(-\frac{2V_{o,k}T_s\mathbf{r}_k^T\cdot\bar{\mathbf{r}}_k}{\sqrt{a^2+b^2}} \right) - \vartheta \tag{18}$$

with $\sin\vartheta = b/\sqrt{a^2+b^2}$ *and* $\cos\vartheta = a/\sqrt{a^2+b^2}$, *where*

$$\begin{aligned} a = &\|\mathbf{r}_k\|^2(y_k - 2v_{ty,k}) + 2x_k v_{tx,k}v_{ty,k} \\ &+ y_k\left[v_{ty,k}^2 - v_{tx,k}^2 + (V_{o,k}T_s)^2\right] \end{aligned} \tag{19}$$

$$\begin{aligned} b = &\|\mathbf{r}_k\|^2(x_k - 2v_{tx,k}) + 2y_k v_{tx,k}v_{ty,k} \\ &+ x_k\left[v_{tx,k}^2 - v_{ty,k}^2 + (V_{o,k}T_s)^2\right] \end{aligned} \tag{20}$$

Proof. For moving target, the relative manoeuvre vector at time step k can be obtained as

$$\begin{aligned} \delta\mathbf{r}_k &= \mathbf{v}_{o,k} - \mathbf{v}_{t,k} \\ &= [V_{o,k}T_s\cos\gamma_{o,k} - v_{tx,k}, V_{o,k}T_s\sin\gamma_{o,k} - v_{ty,k}]^T \end{aligned} \tag{21}$$

Then, the relative position vector at time step $k+1$ is given by

$$\begin{aligned} \mathbf{r}_{k+1} &= \mathbf{r}_k + \delta\mathbf{r}_k \\ &= [x_k + V_{o,k}T_s\cos\gamma_{o,k} - v_{tx,k}, y_k + V_{o,k}T_s\sin\gamma_{o,k} - v_{ty,k}]^T \end{aligned} \tag{22}$$

As depicted in Fig. 2 (b), the separation angle σ between two consecutive relative position vectors is determined by

$$\sigma = \arccos\left(\frac{\mathbf{r}_k^T\cdot\mathbf{r}_{k+1}}{\|\mathbf{r}_k\|\,\|\mathbf{r}_{k+1}\|} \right) \tag{23}$$

Substituting Eq. (23) into Eq. (11) gives

$$J = \frac{1-\cos^2\sigma}{x_{k+1}^2+y_{k+1}^2} = \frac{(x_k y_{k+1} - x_{k+1}y_k)^2}{(x_k^2+y_k^2)\left(x_{k+1}^2+y_{k+1}^2\right)^2} \tag{24}$$

The partial derivative of J with respect to $\gamma_{o,k}$ provides a constraint for identifying the optimal heading as

$$\frac{\partial J}{\partial\gamma_{o,k}} = 0 \tag{25}$$

Substituting (22) into (24) and after some tedious but simple algebraic manipulations, (25) reduces to

$$\begin{aligned} \frac{\partial J}{\partial\gamma_{o,k}} =& 2V_{o,k}T_s\left[(x_k - v_{tx,k} + V_{o,k}T_s\cos\gamma_{o,k})^2 + (y_k - v_{ty,k} + V_{o,k}T_s\sin\gamma_{o,k})^2\right] \\ &\times \frac{x_k(y_k - v_{ty,k} + V_{o,k}T_s\sin\gamma_{o,k}) - y_k(x_k - v_{tx,k} + V_{o,k}T_s\cos\gamma_{o,k})}{\left[(x_k - v_{tx,k} + V_{o,k}T_s\cos\gamma_{o,k})^2 + (y_k - v_{ty,k} + V_{o,k}T_s\sin\gamma_{o,k})^2\right]^4} \\ &\times \Big\{(x_k\cos\gamma_{o,k} + y_k\sin\gamma_{o,k})\left[(x_k - v_{tx,k} + V_{o,k}T_s\cos\gamma_{o,k})^2 + (y_k - v_{ty,k} + V_{o,k}T_s\sin\gamma_{o,k})^2\right] \\ &+ 2\left[x_k(y_k - v_{ty,k} + V_{o,k}T_s\sin\gamma_{o,k}) - y_k(x_k - v_{tx,k} + V_{o,k}T_s\cos\gamma_{o,k})\right] \\ &\times \left[\sin\gamma_{o,k}(x_k - v_{tx,k}) - \cos\gamma_{o,k}(y_k - v_{ty,k})\right]\Big\} \end{aligned} \tag{26}$$

From (26), the solution of $\partial J/\partial\gamma_{o,k} = 0$ can be determined from

$$x_k(y_k - v_{ty,k} + V_{o,k}T_s\sin\gamma_{o,k}) - y_k(x_k - v_{tx,k} + V_{o,k}T_s\cos\gamma_{o,k}) = 0 \tag{27}$$

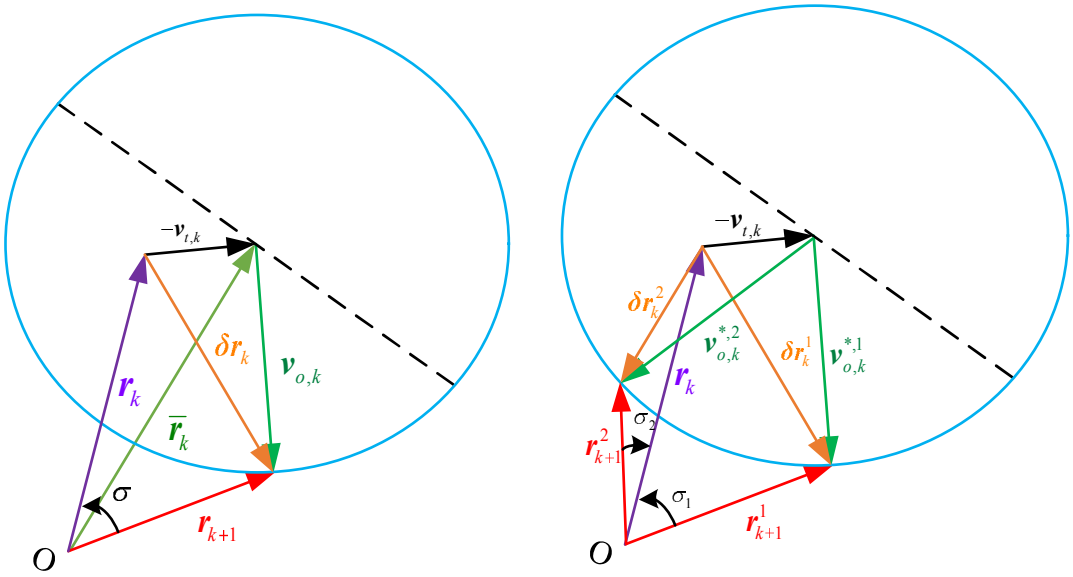

(a) (b)

Fig. 3. (a) Geometric illustration for moving target localisation without turning rate limit in the relative frame. The blue circle determines the maximum permissible region that the observer can travel at current time step. $\bar{\mathbf{r}}_k = \mathbf{r}_k - \mathbf{v}_{t,k}$ is an auxiliary vector utilised in the analysis. (b) Geometric illustration of candidate optimal heading solutions for moving target localisation in the relative frame.

$$\begin{aligned}&(x_k \cos\gamma_{o,k} + y_k \sin\gamma_{o,k}) \left[(x_k - v_{tx,k} + V_{o,k}T_s \cos\gamma_{o,k})^2 + (y_k - v_{ty,k} + V_{o,k}T_s \sin\gamma_{o,k})^2\right] \\ &\quad + 2\left[x_k\left(y_k - v_{ty,k} + V_{o,k}T_s \sin\gamma_{o,k}\right) - y_k\left(x_k - v_{tx,k} + V_{o,k}T_s \cos\gamma_{o,k}\right)\right] \\ &\quad \times \left[\sin\gamma_{o,k}\left(x_k - v_{tx,k}\right) - \cos\gamma_{o,k}\left(y_k - v_{ty,k}\right)\right] = 0\end{aligned} \tag{28}$$

Note that, if $x_k\left(y_k - v_{ty,k} + V_{o,k}T_s \sin\gamma_{o,k}\right) - y_k\left(x_k - v_{tx,k} + V_{o,k}T_s \cos\gamma_{o,k}\right) = 0$, we have $\mathbf{r}_{k+1} = k_2\mathbf{r}_k$, $k_2 \in \mathbb{R}$. This provides zero observability of the target by the angle measurement, which minimises the cost function J. Therefore, this should be excluded from the solution candidates. Together with the fact that the cost function J is continuous, the candidate optimal heading solutions can be obtained from condition (28). Further simplifying (28) yields

$$a\sin\gamma_{o,k} + b\cos\gamma_{o,k} = -2V_{o,k}T_s\mathbf{r}_k^T \cdot \bar{\mathbf{r}}_k \tag{29}$$

Note that

$$a\sin\gamma_{o,k} + b\cos\gamma_{o,k} = \sqrt{a^2+b^2}\sin\left(\gamma_{o,k} + \vartheta\right) \tag{30}$$

Since both a and b are known, the candidate optimal observer heading angle $\gamma_{o,k}^*$ can be directly obtained from (29) and (30) as

$$\gamma_{o,k}^{*,1} = \arcsin\left(-\frac{2V_{o,k}T_s\mathbf{r}_k^T \cdot \bar{\mathbf{r}}_k}{\sqrt{a^2+b^2}}\right) - \vartheta \tag{31}$$

$$\gamma_{o,k}^{*,2} = \pi - \arcsin\left(-\frac{2V_{o,k}T_s\mathbf{r}_k^T \cdot \bar{\mathbf{r}}_k}{\sqrt{a^2+b^2}}\right) - \vartheta \tag{32}$$

□

Remark 8. It follows from Eqs. (31)-(32) that the candidate optimal heading solution with a specific observer velocity $V_{o,k}$ depends on current relative position as well as target's velocity magnitude and its corresponding direction. The geometric illustration of optimal observer manoeuvres for moving target is shown in Fig. 3 (b), where $-\mathbf{v}_{t,k}$ is assumed to be located on the right hand side of $\mathbf{r}_k$. Similar geometry can also be obtained if $-\mathbf{v}_{t,k}$ is located on the left hand side of $\mathbf{r}_k$. From Fig. 3 (b), we can note that both $\gamma_{o,k}^{*,1}$ and $\gamma_{o,k}^{*,2}$ try to reduce the relative range between the observer and the target. In the meantime, these two solutions try to increase the absolute value of the separation angle σ to improve target observability.

Given the robot velocity $V_{o,k}$, Lemma 1 indicates that there exist two candidate heading angle solutions that locally maximise the cost function J, i.e., these two solutions are local maxima. The following lemma analyses the location of these two solutions. Without loss of generality, we assume that $-\mathbf{v}_{t,k}$ is located on the right hand side of $\mathbf{r}_k$, as shown in Fig. 4, in the following analysis. Similar results can also be obtained when $-\mathbf{v}_{t,k}$ is located on the left hand side of $\mathbf{r}_k$.

Lemma 2. *Let Ω_1 be $\triangledown ADE$ that excludes line $\overline{AD}$ and Ω_2 be $\triangledown ABC$ that excludes lines $\overline{AB}$, $\overline{AC}$ (refer to Fig. 4 (a)). Then, the heading solution given by Lemma 1 satisfies $\mathbf{v}_{o,k}^{*,1} \in \Omega_1$ and $\mathbf{v}_{o,k}^{*,2} \in \Omega_2$.*

Proof. The proof of Lemma 2 is given in two steps. The first step proves that the observer manoeuvre vector solutions, given by Lemma 1, are located inside $\triangledown ABD$. The second step shows that $\mathbf{v}_{o,k}^{*,1} \in \Omega_1$ and $\mathbf{v}_{o,k}^{*,2} \in \Omega_2$.

Step 1: As discussed before, the maximisation of J provides a balance between the minimisation of $\|\mathbf{r}_{k+1}\|$ and the maximisation of $|\sin\sigma|$. If the observer manoeuvre vector

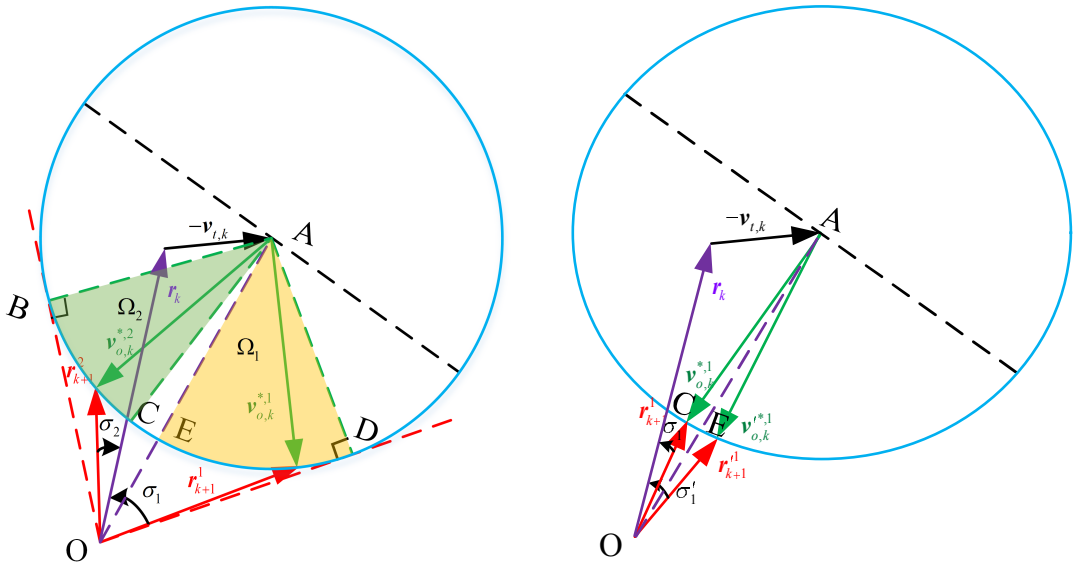

(a) (b)

Fig. 4. Geometric illustration of optimal manoeuvre location in the relative frame. (a) one candidate heading solution $\mathbf{v}^{*,1}_{o,k}$ locates inside sector ADE excluding line $\overline{AD}$ (Ω_1 in the figure) and another candidate heading solution $\mathbf{v}^{*,2}_{o,k}$ locates inside sector ABC excluding lines $\overline{AB}$, $\overline{AC}$ (Ω_2 in the figure). (b) Proof of the fact that that $\mathbf{v}^{*,1}_{o,k} \notin$ sector ACE.

$\mathbf{v}_{o,k}$ coincides with $\overrightarrow{AC}$, one can imply that $\mathbf{r}_{k+1} = \lambda \mathbf{r}_k$ with $\lambda \in \mathbb{R}^+$. This means that both $\mathbf{r}^2_{k+1}$ and $\sin^2\sigma$ achieve their minimum values. Therefore, the proof of step 1 is equivalent to the proof of the fact that the optimal observer manoeuvre vector that maximises $\sin^2\sigma$ is perpendicular to next step relative position vector $\mathbf{r}_{k+1}$.

Consider the cost function $\bar{J} = \sin^2\sigma$. Evaluating the partial derivative of $\bar{J}$ with respect to $\gamma_{o,k}$ gives

$$\begin{aligned}\frac{\partial \bar{J}}{\partial \gamma_{o,k}} =& \frac{2V_{o,k}T_s\left[x_k\left(y_k - v_{ty,k} + V_{o,k}T_s\sin\gamma_{o,k}\right) - y_k\left(x_k - v_{tx,k} + V_{o,k}T_s\cos\gamma_{o,k}\right)\right]}{\left[\left(x_k - v_{tx,k} + V_{o,k}T_s\cos\gamma_{o,k}\right)^2 + \left(y_k - v_{ty,k} + V_{o,k}T_s\sin\gamma_{o,k}\right)^2\right]^2} \\ &\times\Big\{\left(x_k\cos\gamma_{o,k} + y_k\sin\gamma_{o,k}\right)\left[\left(x_k - v_{tx,k} + V_{o,k}T_s\cos\gamma_{o,k}\right)^2 + \left(y_k - v_{ty,k} + V_{o,k}T_s\sin\gamma_{o,k}\right)^2\right] \\ &+\left[x_k\left(y_k - v_{ty,k} + V_{o,k}T_s\sin\gamma_{o,k}\right) - y_k\left(x_k - v_{tx,k} + V_{o,k}T_s\cos\gamma_{o,k}\right)\right] \\ &\times\left[\sin\gamma_{o,k}\left(x_k - v_{tx,k}\right) - \cos\gamma_{o,k}\left(y_k - v_{ty,k}\right)\right]\Big\}\end{aligned} \tag{33}$$

Solving $\partial\bar{J}/\partial\gamma_{o,k} = 0$ gives

$$x_k\left(y_k - v_{ty,k} + V_{o,k}T_s\sin\gamma_{o,k}\right) - y_k\left(x_k - v_{tx,k} + V_{o,k}T_s\cos\gamma_{o,k}\right) = 0 \tag{34}$$

$$\begin{aligned}&\left(x_k\cos\gamma_{o,k} + y_k\sin\gamma_{o,k}\right)\left[\left(x_k - v_{tx,k} + V_{o,k}T_s\cos\gamma_{o,k}\right)^2 + \left(y_k - v_{ty,k} + V_{o,k}T_s\sin\gamma_{o,k}\right)^2\right] \\ &+\left[x_k\left(y_k - v_{ty,k} + V_{o,k}T_s\sin\gamma_{o,k}\right) - y_k\left(x_k - v_{tx,k} + V_{o,k}T_s\cos\gamma_{o,k}\right)\right] \\ &\times\left[\sin\gamma_{o,k}\left(x_k - v_{tx,k}\right) - \cos\gamma_{o,k}\left(y_k - v_{ty,k}\right)\right] = 0\end{aligned} \tag{35}$$

Note that, if $x_k\left(y_k - v_{ty,k} + V_{o,k}T_s\sin\gamma_{o,k}\right) - y_k\left(x_k - v_{tx,k} + V_{o,k}T_s\cos\gamma_{o,k}\right) = 0$, we have $\mathbf{r}_{k+1} = k_2\mathbf{r}_k$, $k_2 \in \mathbb{R}$. This will minimise the cost function $\bar{J}$ since $\sigma = 0$. Therefore, the candidate optimal heading satisfies condition (35). Simplifying Eq. (35) yields

$$\begin{aligned}&\left[\left(x_k - v_{tx,k}\right)\cos\gamma_{o,k} + \left(y_k - v_{ty,k}\right)\sin\gamma_{o,k} + V_{o,k}T_s\right] \\ &\times\left(x_k^2 + y_k^2 - x_k v_{tx,k} - y_k v_{ty,k} + x_k V_{o,k}T_s\cos\gamma_{o,k}\right. \\ &\left.+y_k V_{o,k}T_s\sin\gamma_{o,k}\right) = 0\end{aligned} \tag{36}$$

which is equivalent to

$$\left(\mathbf{r}^T_{k+1}\cdot\mathbf{v}_{o,k}\right)\left(\mathbf{r}^T_k\cdot\mathbf{r}_{k+1}\right) = 0 \tag{37}$$

Since the optimal manoeuvre satisfies the condition that $\mathbf{r}^T_k\cdot\mathbf{r}_{k+1} \neq 0$, the final solution that maximises $\bar{J}$ is given by $\mathbf{r}^T_{k+1}\cdot\mathbf{v}_{o,k} = 0$. This clearly indicates that the optimal observer manoeuvre vector that maximises $\sin^2\sigma$ is perpendicular to next step relative position vector $\mathbf{r}_{k+1}$.

Step 2: Note that if $\mathbf{v}_{o,k} = \overrightarrow{AC}$, the cost function J

achieves the minimum value as $J\left(\overrightarrow{AC}\right)=0$. Therefore, the cost function J monotonically increases when the observer manoeuvre vector $\mathbf{v}_{o,k}$ rotates from $\overrightarrow{AC}$ to $\mathbf{v}_{o,k}^{*,1}$ or to $\mathbf{v}_{o,k}^{*,2}$ since there is no solution $\partial J/\partial\gamma_{o,k}=0$ that is located between $\mathbf{v}_{o,k}^{*,1}$ and $\overrightarrow{AC}$ or between $\mathbf{v}_{o,k}^{*,2}$ and $\overrightarrow{AC}$. This implies that $\mathbf{v}_{o,k}^{*,2}\in\Omega_2$ and $\mathbf{v}_{o,k}^{*,1}$ locates in $\diamondsuit ACD$ that excludes lines $\overline{AC}$, $\overline{AD}$. Now, assume that $\mathbf{v}_{o,k}^{*,1}$ locates inside $\diamondsuit ACE$. Then, according to symmetric property, there always exists a vector $\mathbf{v'}_{o,k}^{*,1}$ such that $\left\|\mathbf{r'}_{k+1}^{1}\right\|=\left\|\mathbf{r}_{k+1}^{1}\right\|$, as shown in Fig. 4 (b). This means that

$$\begin{aligned}J\left(\mathbf{v'}_{o,k}^{*,1}\right)&=\left(\frac{\sin\sigma_1'}{\left\|\mathbf{r'}_{k+1}^{1}\right\|}\right)^2=\left(\frac{\sin\sigma_1'}{\left\|\mathbf{r}_{k+1}^{1}\right\|}\right)^2\\&>\left(\frac{\sin\sigma_1}{\left\|\mathbf{r}_{k+1}^{1}\right\|}\right)^2=J\left(\mathbf{v}_{o,k}^{*,1}\right)\end{aligned}\tag{38}$$

which reveals that $\mathbf{v}_{o,k}^{*,1}\notin\diamondsuit ACE$. Therefore, $\mathbf{v}_{o,k}^{*,1}\in\Omega_1$. □

From Lemma 1, it is clear that the candidate optimal heading command solutions depend on observer's velocity. Now, let us analyse the effect of observer's velocity $V_{o,k}$ on cost function J.

Lemma 3. *The cost function J monotonically increases with respect to the observer's velocity $V_{o,k}$ when $\mathbf{v}_{o,k}\in\Omega_1\cup\Omega_2$.*

Proof. Evaluate the partial derivative of J with respect to $V_{o,k}$ gives

$$\begin{aligned}\frac{\partial J}{\partial V_{o,k}}=&-2T_s\frac{x_k\left(y_k-v_{ty,k}+V_{o,k}T_s\sin\gamma_{o,k}\right)-y_k\left(x_k-v_{tx,k}+V_{o,k}T_s\cos\gamma_{o,k}\right)}{\left[\left(x_k-v_{tx,k}+V_{o,k}T_s\cos\gamma_{o,k}\right)^2+\left(y_k-v_{ty,k}+V_{o,k}T_s\sin\gamma_{o,k}\right)^2\right]^3}\\&\times\left\{\left[\left(x_k-v_{tx,k}+V_{o,k}T_s\cos\gamma_{o,k}\right)^2+\left(y_k-v_{ty,k}+V_{o,k}T_s\sin\gamma_{o,k}\right)^2\right]\left(y_k\cos\gamma_{o,k}-x_k\sin\gamma_{o,k}\right)\right.\\&+2\left[x_k\left(y_k-v_{ty,k}+V_{o,k}T_s\sin\gamma_{o,k}\right)-y_k\left(x_k-v_{tx,k}+V_{o,k}T_s\cos\gamma_{o,k}\right)\right]\\&\left.\times\left[\cos\gamma_{o,k}\left(x_k-v_{tx,k}+V_{o,k}T_s\cos\gamma_{o,k}\right)+\sin\gamma_{o,k}\left(y_k-v_{ty,k}+V_{o,k}T_s\sin\gamma_{o,k}\right)\right]\right\}\end{aligned}\tag{39}$$

Let $\Omega_1=\Omega_3\cup\Omega_4$, where Ω_3 be $\diamondsuit ADF$ that excludes line $\overline{AD}$ and Ω_4 be $\diamondsuit AEF$ that excludes line $\overline{AF}$ (shown in Fig. 5 (a), where line $\overline{AF}$ is parallel to $\mathbf{r}_k$). The following three different conditions are considered.

Condition 1: when $\mathbf{v}_{o,k}\in\Omega_2$, which means that $\mathbf{v}_{o,k}$ is located on the left hand side of $\mathbf{r}_k$, we have

$$y_k\cos\gamma_{o,k}-x_k\sin\gamma_{o,k}<0\tag{40}$$

and $\mathbf{r}_{k+1}$ is located on the left hand side of $\mathbf{r}_k$, e.g.,

$$\begin{aligned}&x_k\left(y_k-v_{ty,k}+V_{o,k}T_s\sin\gamma_{o,k}\right)\\&\quad-y_k\left(x_k-v_{tx,k}+V_{o,k}T_s\cos\gamma_{o,k}\right)>0\end{aligned}\tag{41}$$

Inside $\diamondsuit ABC$ that excludes lines $\overline{AB}$, $\overline{AC}$, it is clear that

$$\mathbf{v}_{o,k}^T\cdot\mathbf{r}_{k+1}<0\tag{42}$$

Note that

$$\begin{aligned}\mathbf{v}_{o,k}^T\cdot\mathbf{r}_{k+1}/\left(V_{o,k}T_s\right)=&\cos\gamma_{o,k}\left(x_k-v_{tx,k}+V_{o,k}T_s\cos\gamma_{o,k}\right)\\&+\sin\gamma_{o,k}\left(y_k-v_{ty,k}+V_{o,k}T_s\sin\gamma_{o,k}\right)\end{aligned}\tag{43}$$

Substituting Eqs. (40)-(43) into Eq. (39) yields $\partial J/\partial V_{o,k}>0$. This implies that when $\mathbf{v}_{o,k}\in\Omega_2$, the cost function J monotonically increases with the increase of observer's velocity $V_{o,k}$.

Condition 2: When $\mathbf{v}_{o,k}\in\Omega_3$, one can imply that

$$y_k\cos\gamma_{o,k}-x_k\sin\gamma_{o,k}\geq 0\tag{44}$$

where the equality holds when $\mathbf{v}_{o,k}=\overrightarrow{AF}$, and $\mathbf{r}_{k+1}$ is located on the right hand side of $\mathbf{r}_k$, e.g.,

$$\begin{aligned}&x_k\left(y_k-v_{ty,k}+V_{o,k}T_s\sin\gamma_{o,k}\right)\\&\quad-y_k\left(x_k-v_{tx,k}+V_{o,k}T_s\cos\gamma_{o,k}\right)<0\end{aligned}\tag{45}$$

Inside $\diamondsuit ADE$ that excludes line $\overline{AD}$, it is clear that

$$\mathbf{v}_{o,k}^T\cdot\mathbf{r}_{k+1}<0\tag{46}$$

Substituting Eqs. (43)-(46) into Eq. (39) yields $\partial J/\partial V_{o,k}>0$. This implies that when $\mathbf{v}_{o,k}\in\Omega_3$, the cost function J monotonically increases with the increase of observer's velocity $V_{o,k}$.

Condition 3: When $\mathbf{v}_{o,k}\in\Omega_4$, the geometric illustration is presented in Fig. 5 (b), where line $\overline{GH}$ is parallel to $\mathbf{r}_k$. In this condition, it is clear that $\mathbf{v}_{o,k}$ is located on the left hand side of $\mathbf{r}_k$ and $\mathbf{r}_{k+1}$ is located on the right hand side of $\mathbf{r}_k$. Therefore, we have

$$-\left\|\mathbf{r}_k\right\|\left\|\mathbf{v}_{o,k}\right\|\sin\varphi=V_{o,k}T_s\left(y_k\cos\gamma_{o,k}-x_k\sin\gamma_{o,k}\right)\tag{47}$$

$$\begin{aligned}-\left\|\mathbf{r}_k\right\|\left\|\mathbf{r}_{k+1}\right\|\sin\sigma=&x_k\left(y_k-v_{ty,k}+V_{o,k}T_s\sin\gamma_{o,k}\right)\\&-y_k\left(x_k-v_{tx,k}+V_{o,k}T_s\cos\gamma_{o,k}\right)\end{aligned}\tag{48}$$

Substituting Eqs. (47) and (48) into Eq. (39) and after some algebraic manipulations results in

$$\frac{\partial J}{\partial V_{o,k}}=-2\frac{\left\|\mathbf{r}_k\right\|^2\left\|\mathbf{v}_{o,k}\right\|\sin\sigma}{V_{o,k}\left\|\mathbf{r}_{k+1}\right\|^3}\left(\sin\varphi+2\sin\sigma\cos\theta\right)\tag{49}$$

From Fig. 5 (b), one can easily verify that

$$2\sin\sigma\cos\theta=-\sin\left(2\sigma-\varphi\right)-\sin\varphi\tag{50}$$

Therefore, we have

$$\sin\varphi+2\sin\sigma\cos\theta=-\sin\left(2\sigma-\varphi\right)\tag{51}$$

From Fig. 5 (b), one can note that φ monotonically increases and σ monotonically decreases when $\mathbf{v}_{o,k}$ rotates from $\overrightarrow{AF}$ to

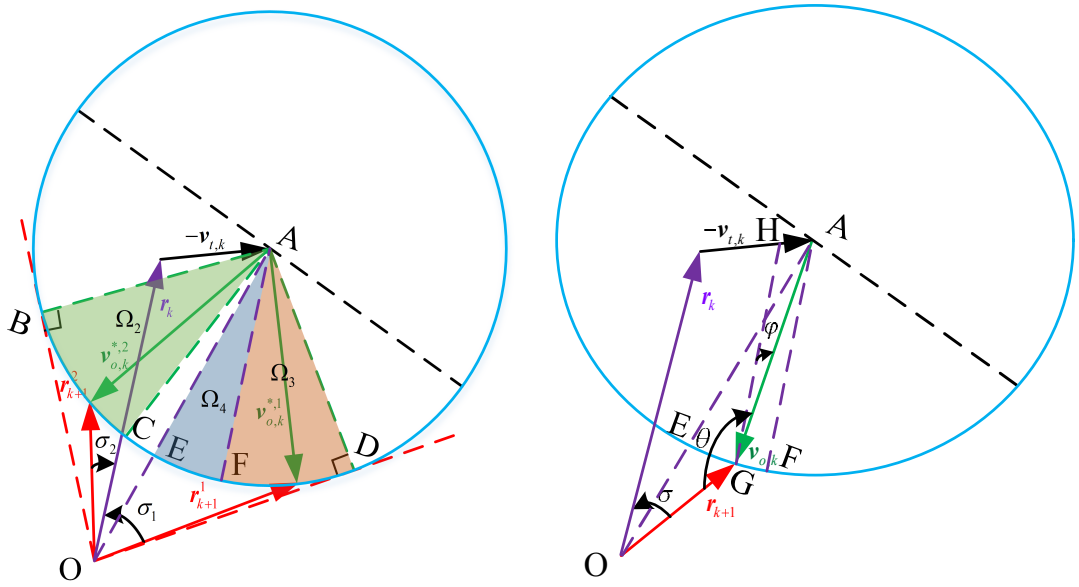

(a) (b)

Fig. 5. Geometric illustration for the proof of Lemma 3 in the relative frame. (a) Three cases are considered to prove J is a monotonically increasing function with respect to $V_{o,k}$ when $\mathbf{v}_{o,k} \in \Omega_2, \Omega_3, \Omega_4$ with Ω_3 being sector ADF that excludes line $\overline{AD}$ and Ω_4 being sector AEF that excludes line $\overline{AF}$. In this figure, line $\overline{AF}$ is parallel to $\mathbf{r}_k$. (b) Proof of the geometric relationship shown in Eq. (50) when $\mathbf{v}_{o,k} \in \Omega_4$. In this figure, both lines $\overline{AF}$ and $\overline{GH}$ are parallel to $\mathbf{r}_k$.

$\overrightarrow{AE}$. Define $\bar{\sigma} = \sigma\left(\overrightarrow{AF}\right)$ and $\hat{\sigma} = \sigma\left(\overrightarrow{AE}\right)$. Then, we have $\hat{\sigma} \leq 2\sigma - \varphi \leq 2\bar{\sigma}$. Note that $0 < \sigma < \pi/2$, as discussed before, one can imply that $0 < 2\sigma - \varphi < \pi$, which means $\sin(2\sigma - \varphi) > 0$. With this in mind and substituting Eq. (51) into Eq. (49) gives $\partial J/\partial V_{o,k} > 0$. This implies that when $\mathbf{v}_{o,k} \in \Omega_4$, the cost function J monotonically increases with the increase of observer's velocity $V_{o,k}$. Finally, combining Conditions 1-3 leads to the proof of Lemma 3. □

By using the results of Lemmas 1-3, the solution of *CTO*$_2$ is obtained in Theorem 1.

Theorem 1. *The optimal observer manoeuvre, without any heading constraints, that maximises cost function J is given by* $\mathbf{v}_{o,k} = \left[V_{o,\max}T_s\cos\gamma^*_{o,k}, V_{o,\max}T_s\sin\gamma^*_{o,k}\right]^T$ *where* $\gamma^*_{o,k} = \max_{\gamma_{o,k}\in\{\gamma^{*,1}_{o,k},\gamma^{*,2}_{o,k}\}} J(\gamma_{o,k})$ *with*

$$\gamma^{*,1}_{o,k} = \arcsin\left(-\frac{2V_{o,\max}T_s\mathbf{r}_k^T\cdot\bar{\mathbf{r}}_k}{\sqrt{a^2+b^2}}\right) - \vartheta \tag{52}$$

$$\gamma^{*,2}_{o,k} = \pi - \arcsin\left(-\frac{2V_{o,\max}T_s\mathbf{r}_k^T\cdot\bar{\mathbf{r}}_k}{\sqrt{a^2+b^2}}\right) - \vartheta \tag{53}$$

Here, $\sin\vartheta = b/\sqrt{a^2+b^2}$ *and* $\cos\vartheta = a/\sqrt{a^2+b^2}$, *where*

$$\begin{aligned} a = &\|\mathbf{r}_k\|^2(y_k - 2v_{ty,k}) + 2x_k v_{tx,k}v_{ty,k} \\ &+ y_k\left[v^2_{ty,k} - v^2_{tx,k} + (V_{o,\max}T_s)^2\right] \end{aligned} \tag{54}$$

$$\begin{aligned} b = &\|\mathbf{r}_k\|^2(x_k - 2v_{tx,k}) + 2y_k v_{tx,k}v_{ty,k} \\ &+ x_k\left[v^2_{tx,k} - v^2_{ty,k} + (V_{o,\max}T_s)^2\right] \end{aligned} \tag{55}$$

Proof. From Lemmas 1-3, the proof of Theorem 1 is straightforward. □

Remark 9. Theorem 1 shows that cost function J is maximised when the robot moves with its maximum velocity $V_{o,max}$. However, it is often not desirable to set the robot velocity as its maximum permissible value due to physical and operational reasons such as endurance consideration. In practice, the robot velocity is usually predefined in consideration of those constraints and mission objectives. Therefore, we limit the following analysis to the case where the robot velocity is constant as $V_{o,k} = V_o$.

B. A Special Case: Stationary Target Localisation

For stationary target, we have $\mathbf{r}_k = \bar{\mathbf{r}}_k$ and

$$a = \left[\|\mathbf{r}_k\|^2 + (V_oT_s)^2\right] y_k \tag{56}$$

$$b = \left[\|\mathbf{r}_k\|^2 + (V_oT_s)^2\right] x_k \tag{57}$$

Then, condition given in (29) becomes

$$\sin(\gamma_{o,k} + \beta) = -\frac{2V_oT_s\|\mathbf{r}_k\|}{\|\mathbf{r}_k\|^2 + (V_oT_s)^2} \tag{58}$$

where $\sin\beta = x_k/\|\mathbf{r}_k\|$, $\cos\beta = y_k/\|\mathbf{r}_k\|$. Therefore, the optimal heading angle at time step k for stationary target localisation is given by

$$\gamma^{*,1}_{o,k} = \arcsin\left(-\frac{2V_oT_s\|\mathbf{r}_k\|}{\|\mathbf{r}_k\|^2 + (V_oT_s)^2}\right) - \beta \tag{59}$$

$$\gamma^{*,2}_{o,k} = \pi - \arcsin\left(-\frac{2V_oT_s\|\mathbf{r}_k\|}{\|\mathbf{r}_k\|^2 + (V_oT_s)^2}\right) - \beta \tag{60}$$

The geometric interpretation of optimal manoeuvres is shown in Fig. 6. Unlike the moving target case, the two

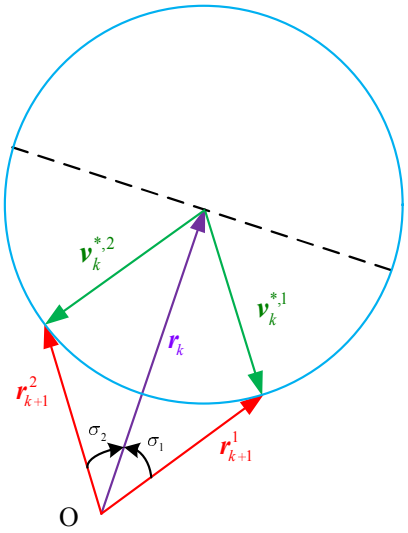

Fig. 6. Geometric interpretation of optimal manoeuvres for stationary target in the relative frame with $\sigma_1 = \sigma_2$ and $\left\|\mathbf{r}_{k+1}^1\right\| = \left\|\mathbf{r}_{k+1}^2\right\|$.

candidate solutions $\gamma_{o,k}^{*,1}$ and $\gamma_{o,k}^{*,2}$ are symmetric with respect to $\mathbf{r}_k$.

For moving target, it is clear from Fig. 3 (b) that the change of the relative distance depends on target movement. However, when localising a stationary target, the relative distance is monotonically decreasing as time goes. Also, the rate of the relative range change is proportional to the square of the observer velocity V_o^2 and the sampling time T_s, but inversely proportional to the current relative range $\|\mathbf{r}_k\|$. This result is given by the following proposition.

Proposition 1. *For stationary target localisation, the rate of the relative range between the observer and the target generated by the obtained optimal manoeuvre is given by*

$$\frac{d\left\|\mathbf{r}_k\right\|}{dt} = -\frac{3V_o^2 T_s}{2\left\|\mathbf{r}_k\right\|} \tag{61}$$

Proof. By definition, the rate of the relative range is determined by

$$\begin{aligned}\frac{d\|\mathbf{r}_k\|}{dt} &= \frac{\|\mathbf{r}_{k+1}\|-\|\mathbf{r}_k\|}{T_s} \\ &= \frac{\sqrt{\|\mathbf{r}_k\|^2+(V_oT_s)^2+2V_oT_s\left(x_k\cos\gamma_{o,k}^*+y_k\sin\gamma_{o,k}^*\right)}-\|\mathbf{r}_k\|}{T_s}\end{aligned} \tag{62}$$

Substituting Eq. (58) into Eq.(62) yields

$$\begin{aligned}\frac{d\left\|\mathbf{r}_k\right\|}{dt} &= \frac{\sqrt{\left\|\mathbf{r}_k\right\|^2+(V_oT_s)^2-\frac{4(V_oT_s)^2\|\mathbf{r}_k\|^2}{\|\mathbf{r}_k\|^2+(V_oT_s)^2}}-\left\|\mathbf{r}_k\right\|}{T_s} \\ &= \frac{\sqrt{\left\|\mathbf{r}_k\right\|^2+\frac{(V_oT_s)^2\left[(V_oT_s)^2-3\|\mathbf{r}_k\|^2\right]}{\|\mathbf{r}_k\|^2+(V_oT_s)^2}}-\left\|\mathbf{r}_k\right\|}{T_s}\end{aligned} \tag{63}$$

Since T_s is small, we have

$$\begin{aligned}\frac{d\left\|\mathbf{r}_k\right\|}{dt} &\approx \frac{\sqrt{\left\|\mathbf{r}_k\right\|^2-3(V_oT_s)^2}-\left\|\mathbf{r}_k\right\|}{T_s} \\ &= \frac{\left\|\mathbf{r}_k\right\|\sqrt{1-\frac{3(V_oT_s)^2}{\|\mathbf{r}_k\|^2}}-\left\|\mathbf{r}_k\right\|}{T_s} \\ &\approx \frac{\left\|\mathbf{r}_k\right\|\left(1-\frac{3}{2}\frac{(V_oT_s)^2}{\|\mathbf{r}_k\|^2}\right)-\left\|\mathbf{r}_k\right\|}{T_s} \\ &= -\frac{3V_o^2T_s}{2\left\|\mathbf{r}_k\right\|}\end{aligned} \tag{64}$$

which clearly indicates the that relative distance is monotonically decreasing as time goes. □

C. Optimal Manoeuvre with Heading Constraint

Theorem 1 reveals that, given the observer velocity, there might exist two optimal heading angles, $\gamma_{o,k}^{*,1}$ and $\gamma_{o,k}^{*,2}$, which generate the same value of cost function for the observer to minimise target localisation error. From the standpoint of real application, it is desirable to avoid zigzag heading angle change to maintain the physical constraints. Therefore, it is necessary to consider physical constraints and select one manoeuvre vector respecting those constraints, when implementing Theorem 1 in practice. This subsection will show how the heading angle constraint (2) can be embedded into the proposed optimal solution.

Let $\gamma_{o,k-1}^*$ be the optimal heading angle at the previous time step. Without loss of generality, assume that $\gamma_{o,k}^{*,1}$ is closer to $\gamma_{o,k-1}^*$ than $\gamma_{o,k}^{*,2}$, as shown in Fig. 7, e.g., $\left|\gamma_{o,k}^{*,1}-\gamma_{o,k-1}^*\right| \leq \left|\gamma_{o,k}^{*,2}-\gamma_{o,k-1}^*\right|$. Then, the solution of CTO_1 is given by the following theorem.

Theorem 2. *Let Ξ be $\heartsuit ADE$ (shown in Fig. 7). Then, we have the following results:*

(1) if $\gamma_{o,k}^{*,1} \in \Xi$ and $\gamma_{o,k}^{*,2} \in \Xi$ (refer to Fig. 7 (a)), then, the optimal observer heading angle $\gamma_{o,k}^*$ considering turning rate constraint is determined as

$$\gamma_{o,k}^* = \begin{cases} \gamma_{o,k}^{*,1}, & \text{if } J\left(\gamma_{o,k}^{*,1}\right) = J\left(\gamma_{o,k}^{*,2}\right) \\ \max\limits_{\gamma_{o,k}\in\left\{\gamma_{o,k}^{*,1},\gamma_{o,k}^{*,2}\right\}} J\left(\gamma_{o,k}\right), & \text{otherwise} \end{cases} \tag{65}$$

(2) if only $\gamma_{o,k}^{*,1} \in \Xi$ (refer to Fig. 7 (b)), then, the optimal observer heading angle $\gamma_{o,k}^*$ considering turning rate constraint is determined as

$$\gamma_{o,k}^* = \max_{\gamma_{o,k}\in\left\{\gamma_{o,k}^{*,1},\bar{\gamma}_{o,k}^{*,1},\bar{\gamma}_{o,k}^{*,2}\right\}} J\left(\gamma_{o,k}\right) \tag{66}$$

where $\bar{\gamma}_{o,k}^{*,1} = \gamma_{o,k-1}^* - \gamma_{\max}$ and $\bar{\gamma}_{o,k}^{*,2} = \gamma_{o,k-1}^* + \gamma_{\max}$.

(3) if $\gamma_{o,k}^{*,1} \notin \Xi$ (refer to Fig. 7 (c)), then, the optimal observer heading angle $\gamma_{o,k}^*$ considering turning rate constraint is determined as

$$\gamma_{o,k}^* = \max_{\gamma_{o,k}\in\left\{\bar{\gamma}_{o,k}^{*,1},\bar{\gamma}_{o,k}^{*,2}\right\}} J\left(\gamma_{o,k}\right) \tag{67}$$

Proof. When $\gamma_{o,k}^{*,1} \in \Xi$ and $\gamma_{o,k}^{*,2} \in \Xi$, the optimal heading angle that maximises cost function J is obviously given by

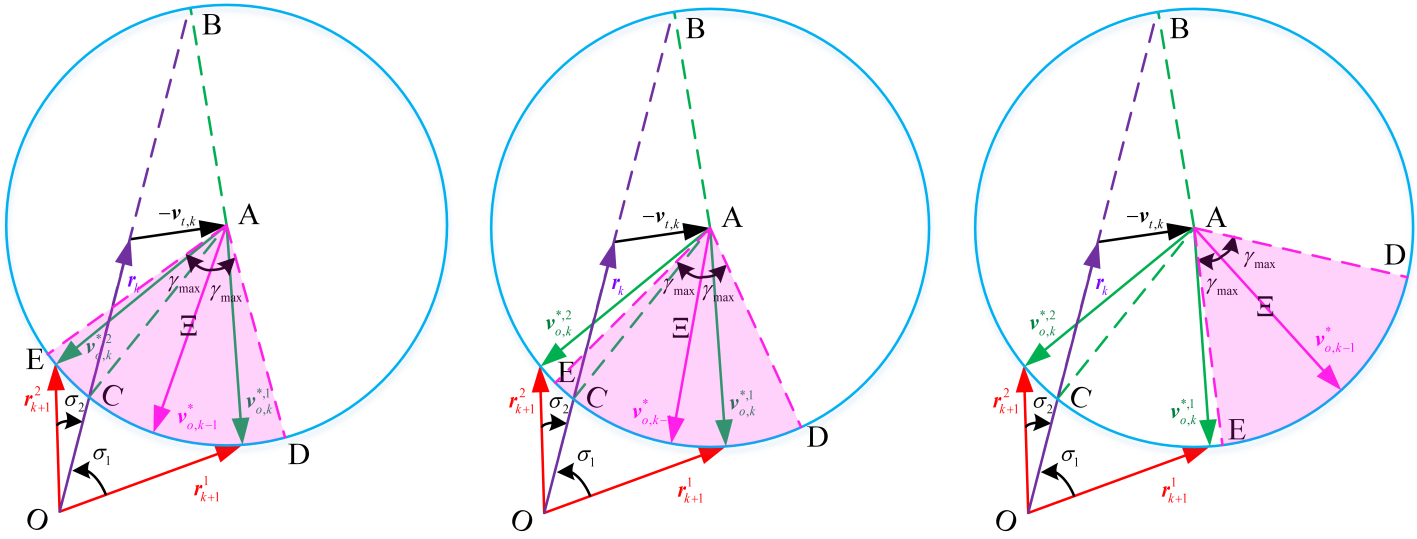

(a) (b) (c)

Fig. 7. Geometric illustration for moving target localisation with turning rate limit in the relative frame. The magenta sector ADE, denoted as Ξ, quantifies the maximum permissible movement region of the robot at current time instant. (a) Case 1: both $\gamma^{*,1}_{o,k}$ and $\gamma^{*,2}_{o,k}$ are located inside sector ADE. (b) Case 2: only $\gamma^{*,1}_{o,k}$ is located inside sector ADE. (c) Case 3: $\gamma^{*,1}_{o,k}$ is located outside sector ADE.

$\gamma^*_{o,k} = \max_{\gamma_{o,k} \in \left\{\gamma^{*,1}_{o,k}, \gamma^{*,2}_{o,k}\right\}} J\left(\gamma_{o,k}\right)$. If these two candidate heading solutions provide the same level of optimality, we then choose the solution which is closer to the previous heading angle to avoid large heading change, as shown in Eq. (65).

Lemma 1 indicates that if $\mathbf{v}_{o,k} = \overrightarrow{AB}$ or $\mathbf{v}_{o,k} = \overrightarrow{AC}$, the cost function J achieves the minimum value as $J\left(\overrightarrow{AB}\right) = 0$ and $J\left(\overrightarrow{AC}\right) = 0$. Also, when $\mathbf{v}_{o,k} = \mathbf{v}^{*,1}_{o,k}$ or $\mathbf{v}_{o,k} = \mathbf{v}^{*,2}_{o,k}$, the cost function J is locally maximised. Therefore, the cost function J monotonically decreases when the observer manoeuvre vector $\mathbf{v}_{o,k}$ rotates from $\mathbf{v}^{*,1}_{o,k}$ (or $\mathbf{v}^{*,2}_{o,k}$) to $\overrightarrow{AB}$ or to $\overrightarrow{AC}$ since there is no solution $\partial J/\partial \gamma_{o,k} = 0$ that is located between $\mathbf{v}^{*,1}_{o,k}$ (or $\mathbf{v}^{*,2}_{o,k}$) and $\overrightarrow{AB}$ or $\mathbf{v}^{*,1}_{o,k}$ (or $\mathbf{v}^{*,2}_{o,k}$) and $\overrightarrow{AC}$. This leads to the proof of results (2) and (3) in Theorem 2. □

Remark 10. Note that when $\gamma^{*,2}_{o,k}$ is closer to $\gamma^*_{o,k-1}$ than $\gamma^{*,1}_{o,k}$, i.e., $\left|\gamma^{*,1}_{o,k} - \gamma^*_{o,k-1}\right| > \left|\gamma^{*,2}_{o,k} - \gamma^*_{o,k-1}\right|$, similar results as shown in Theorem 2 can also be obtained.

D. Algorithm Summary

By summarising the results presented in Sec. IV A and Sec. IV C, the proposed optimal trajectory optimisation algorithm for target localisation with bearing-only measurement is summarised in Algorithm 1.

Algorithm 1 Optimal Trajectory Optimisation for Target Localisation with Bearing-Only Measurement

Input: Estimated target position vector $\mathbf{r}_{t,k}$, estimated target manoeuvre vector $\mathbf{v}_{t,k}$, previous observer manoeuvre vector $\mathbf{v}_{o,k-1}$, maximum allowable heading angle change $\gamma_{\max}$
Output: Optimal observer heading angle $\gamma^*_{o,k}$

Calculate the candidate optimal heading angles $\gamma^{*,1}_{o,k}$ and $\gamma^{*,2}_{o,k}$ using Eqs. (17) and (18)
if $\left|\gamma^{*,1}_{o,k} - \gamma^*_{o,k-1}\right| \leq \left|\gamma^{*,2}_{o,k} - \gamma^*_{o,k-1}\right|$ **then**
    $\bar{\gamma}^*_{o,k} = \gamma^{*,1}_{o,k}$
else
    $\bar{\gamma}^*_{o,k} = \gamma^{*,2}_{o,k}$
end if
if $\left|\gamma^{*,1}_{o,k} - \gamma^*_{o,k-1}\right| \leq \gamma_{\max}$ and $\left|\gamma^{*,2}_{o,k} - \gamma^*_{o,k-1}\right| \leq \gamma_{\max}$ **then**
    $\gamma^*_{o,k}$ is given by Eq. (65)
else if $\left|\bar{\gamma}^*_{o,k} - \gamma^*_{o,k-1}\right| \leq \gamma_{\max}$ **then**
    $\gamma^*_{o,k}$ is given by Eq. (66)
else
    $\gamma^*_{o,k}$ is given by Eq. (67)
end if

E. Observability Analysis Under the Proposed Algorithm

In the development of the proposed algorithm, the assumption that $\mathbf{r}_k$ is available is utilised in trajectory optimisation. However, the information on $\mathbf{r}_k$ is extracted from Kalman filter in practice. This means that only when the system is observable, $\mathbf{r}_k$ is available to the observer. For this reason, this subsection will analyse the system observability under the proposed approach using geometric concepts. The primary objective of observability analysis is to find out whether or not $\mathbf{r}_k$ can be uniquely determined within a finite time period from time instant k onward. The results are given in the following proposition.

Proposition 2. *For constant-manoeuvring target, the target observability is ensured under the proposed algorithm.*

Proof. In [13], the authors revealed that the necessary and sufficient condition to guarantee system observability for

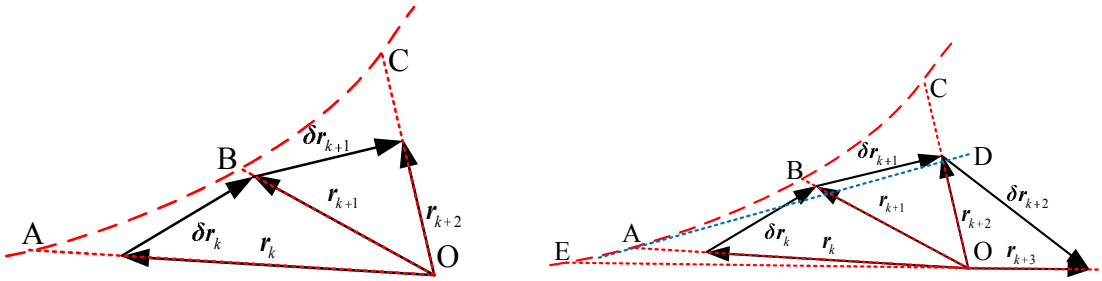

(a) (b)

Fig. 8. (a) Geometric interpretation of the necessary and sufficient observability condition for three consecutive time steps for constant-manoeuvring target with bearing-only measurement. (b) Geometric interpretation utilised in the proof of Proposition 2. In (b), line $\overline{AD}$ is the tangential line of quadratic curve AC at point A.

constant-manoeuvring target with bearing-only measurement is given by

$$\mathbf{r}(t) \neq \lambda(t) \begin{bmatrix} a_{11} + a_{12}\Delta t + a_{13}\frac{\Delta t^2}{2} \\ a_{21} + a_{22}\Delta t + a_{23}\frac{\Delta t^2}{2} \end{bmatrix} \tag{68}$$

for some $t \in (t_0, t_f]$ with t_0 being the initial time, where $\Delta t = t - t_0$ and $\lambda(t)$ is an arbitrary scalar function. The coefficients a_{ij} in Eq. (68) are arbitrary constants but not all zero.

According to condition (68), if the system is unobservable, there exists a quadratic curve such that the relative position vector has a linear relationship with the quadratic curve. A geometric illustration of condition (68) for three consecutive time steps is presented in Fig. 8. If the system is unobservable, there exist an arbitrary scalar function $\lambda(t)$ and a quadratic curve AC such that $\mathbf{r}_k = \lambda(t_k)\overrightarrow{OA}$, $\mathbf{r}_{k+1} = \lambda(t_{k+1})\overrightarrow{OB}$ and $\mathbf{r}_{k+2} = \lambda(t_{k+2})\overrightarrow{OC}$ locates on the quadratic curve AC. It is clear that $\sigma = 0$ is a special case that violates condition (68).

Define $r_x(t) = a_{11} + a_{12}\Delta t + a_{13}\frac{\Delta t^2}{2}$ and $r_y(t) = a_{21} + a_{22}\Delta t + a_{23}\frac{\Delta t^2}{2}$. Due to the property of quadratic polynomials, there exists a certain time instant $t_* > t_0$ such that both $r_x(t)$ and $r_y(t)$ are monotonic functions when $t > t_*$. Without loss of generality, we assume that $t_k > t_*$. From previous analysis, we know that the proposed algorithm generates a unique solution that forces the relative position vector rotate clockwise or anti-clockwise around the target. Without loss of generality, the clockwise rotation direction (as shown in Fig. 8 (a)) is utilised in the following analysis. With this in mind, one can imply that there exists a certain time instant (assuming this occurs at time step $k+3$ for simplicity) such that $\mathbf{r}_{k+3}$ is located on the right hand of $\overrightarrow{AD}$, as shown in Fig. 8 (b), where line $\overline{OD}$ is the tangential line of quadratic curve AC at point A. Since quadratic curves are convex, it is easy to verify that the only intersection point between quadratic curve AC and $\mathbf{r}_{k+3}$ is E. This apparently violates the condition that $r_x(t)$ and $r_y(t)$ are monotonic when $t > t_*$. Therefore, $\forall t_k$, there exists some $t \in (t_k, t_f]$ such that condition (68) is satisfied. This means that target is observable under the proposed approach. □

V. Simulation Studies

In this section, estimator-in-the-loop simulations are performed to validate the proposed optimal trajectory optimisation algorithm. To illustrate and evaluate performance characteristics, the proposed algorithm was tested and compared with the algorithms proposed in [14] and [42], via extensive simulations. This section presents representative results for three typical tracking scenarios.

A. Simulation Setup

In the given scenarios, an aerial robot tracks a ground target using bearing-only measurement. The robot is assumed to be flying with a constant velocity $V_o = 20m/s$. The initial position of the robot is $(20m, 50m)$ and the target initially locates at $(0m, 0m)$. The turning rate of the robot is constrained by $\omega_{\max} = 1.5rad/s$ and the sampling time is set as $T_s = 0.1s$. The angle measurement noise ε is assumed to be zero-mean white Gaussian as $\mathcal{N}(\varepsilon; 0, \sigma_\varepsilon^2)$ with $\sigma_\varepsilon = 0.5°$. In the simulation scenarios, three different types of targets are considered: (1) Case 1: target is stationary; (2) Case 2: target moves in a straight line with constant velocity $V_t = 5.83m/s$ and constant heading $\gamma_t = 0.54rad$; and (3) Case 3: target moves with constant velocity $V_t = 10m/s$, constant turning rate $\dot{\gamma}_t = \pi/24rad/s$ and initial heading $\gamma_{t,1} = 0°$.

To implement the proposed trajectory optimisation algorithm, the required information on target position and velocity are estimated using the well-known extended Kalman filter (EKF). In EKF design, as we utilise the piece-wise non-manoeuvring assumption in algorithm development, the standard constant velocity (CV) model is utilised as the target dynamics for prediction. Let $\mathbf{x}_k = [x_{t,k}, \dot{x}_{t,k}, y_{t,k}, \dot{y}_{t,k}]^T$, the state transition of CV model is determined by

$$\mathbf{x}_k = F_{CV}\mathbf{x}_{k-1} + G_{CV}w_{k-1} \tag{69}$$

with

$$F_{CV} \triangleq \mathbb{I}_{2\times 2} \otimes \begin{bmatrix} 1 & T_s \\ 0 & 1 \end{bmatrix}, \quad G_{CV} \triangleq \begin{bmatrix} T_s^2/2 \\ T_s \\ T_s^2/2 \\ T_s \end{bmatrix} \tag{70}$$

where $\mathbb{I}_{2\times 2}$ denotes the 2×2 identity matrix, and $w_k \sim \mathcal{N}(\cdot; 0, \sigma_v^2)$ the Gaussian process noise with $\sigma_v = 0.5m/s^2$.

Since the estimation error covariance matrix is positive definite, its quadratic form constitutes a hyper uncertainty ellipsoid that determines the error distribution and the axes of ellipsoids are defined by the eigenvalues of the error covariance matrix. Therefore, the volume of the uncertainty ellipsoid can be used as a meaningful performance metric to quantify the estimation accuracy. Let P denote the target position error covariance, the one sigma area of the uncertainty ellipsoid is determined as

$$A_{1\sigma} = \pi\sqrt{|P|} \tag{71}$$

Note that the FIM is inversely related with the error covariance matrix. Thus, the minimisation of the volume of the uncertainty ellipsoid can be achieved by maximising the determinant of FIM. This means that the robot trajectory that generates higher observability of the target has higher value of $|F|$. Therefore, we utilise the determinant of FIM as a metric to check the performance in simulations. Note that the FIM can be calculated in a recursive way as described in [44].

B. Comparison with [14]

By utilising a lower bound of the determinant of the incremental of FIM as a cost function, the authors in [14] suggested a solution to minimise estimation error for bearing-only measurement navigation. This subsection compares the proposed approach with [42] to demonstrate the advantages of the proposed geometric measure. The one-step optimal observer manoeuvre that maximises $\hat{J}$ is obtained through the Genetic Algorithm (GA) solver from Matlab Optimization Toolbox since it is difficult to find analytical solutions that maximise $\hat{J}$. For fair comparison, the robot heading constraint is also embedded into the GA solver. It should be pointed out [14] never considered the physical constraints in the implementation. Note that for one-step trajectory optimisation, maximising $(\sigma/\|\mathbf{r}_k\|)^2$ is equivalent to maximise the absolute value of the separation angle between two consecutive time steps since $\|\mathbf{r}_k\|$ is known.

The comparison results obtained by these two different algorithms for all three cases are shown in Fig. 9. The first row in Fig. 9 provides the robot and target trajectories for these three cases. From these three figures, it can be noted that the robot trajectories generated by the proposed algorithm always locate inside the robot trajectories obtained by maximising $\hat{J}$. This reveals that the proposed algorithm provides a proper balance between maximising the absolute value of the separation angle and the minimisation of the relative range, whereas maximising $\hat{J}$ only maximises the absolute value of the separation angle. The corresponding determinant of FIM obtained from two different algorithms are depicted in the second row of Fig. 9. It is clear that the proposed algorithm generates higher value of $|F_k|$ as time goes, demonstrating that optimisation of the proposed geometric metric (11) generates higher system observability than that of maximising $\hat{J}$. Since the one sigma volume of the uncertainty ellipsoid $A_{1\sigma}$ is inversely proportional to $|F|$, the proposed trajectory optimisation algorithm is expected to generate smaller error ellipsoid.

TABLE I
RMSE COMPARISONS OVER1000 MONTE-CARLO RUNS.

	Metric	Case 1	Case 2	Case 3
Optimising $\hat{J}$ [14]	Mean	$1.6259m$	$1.8264m$	$2.5933m$
	Std	$0.4171m$	$0.5852m$	$0.6319m$
Optimising J (11)	Mean	$1.5027m$	$1.5408m$	$2.0562m$
	Std	$0.4059m$	$0.5466m$	$0.6412m$

For better illustration, Monte-Carlo simulations are carried out to validate the proposed approach. In each Monte-Carlo run, the robot's initial position $(x_{o,1}, y_{o,1})$ is randomly sampled from uniform distributions as $x_{o,1} \sim \mathcal{U}(-40m, 40m)$ and $y_{o,1} \sim \mathcal{U}(-40m, 40m)$. The standard deviation of the measurement noise σ_ε at each Monte-Carlo run is also randomly sampled from uniform distribution as $\sigma_\varepsilon \sim \mathcal{U}(0.5^\circ, 2^\circ)$. The time averaged and standard deviation (Std) of root-mean-square errors (RMSEs) over 1000 Monte-Carlo runs obtained from different algorithms for the aforementioned three cases are summarised in Table I. From this table, it is clear the proposed analytical algorithm that maximising J yields improved localisation performance than numerically maximising $\hat{J}$, especially when target is moving. This coincides with the results shown in the second row of Fig. 9. The Monte-Carlo simulation results also reveal that minimising the relative range between the robot and the target provides the possibility to reduce the estimation uncertainty, which complies with the geometric concept discussed before. To further demonstrate that maximising $\hat{J}$ is indeed different from J, t-test between these two approaches is performed with 5% significance level and the result is $h = 1$ for all three cases. This reveals that optimising these two different performance metrics is statistically different. Also note from Table I that both algorithms generate comparable level of standard deviation over large number of Monte-Carlo simulations. This can be attributed to the fact we consider the physical turning rate limit in implementing both algorithms, which means the generated optimal heading command is unique and consistent.

C. Comparison with [42]

By minimising the trace of the error covariance at next time step, an analytical optimal trajectory optimisation algorithm for target localisation with bearing-only measurement is proposed in [42], where the control input is robot's position. However, since physical constraints of the robot are not rigorously considered in this work, the solution might become infeasible. This subsection compares the proposed approach with [42] to demonstrate the importance of considering turning rate constraint.

The simulation results obtained by these two different algorithms for two sample runs of case 3 are depicted in Fig. 10, in which each row corresponds to one sample run. It is clear from the first column of Fig. 10 that analytical solution proposed in [42] finds multiple candidate optimal robot trajectories. Numerically picking one of them inevitably generates zigzag form motion trajectory, thus resulting in large heading angle change. This can be noted from the blue peaks of robot turning rate in the third column of Fig. 10. As a comparison, by

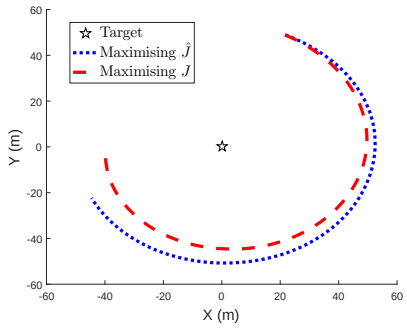

(a) Robot and target trajectories of case 1

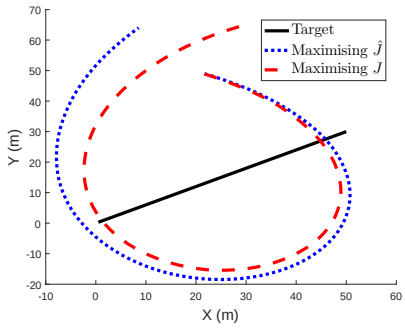

(b) Robot and target trajectories of case 2

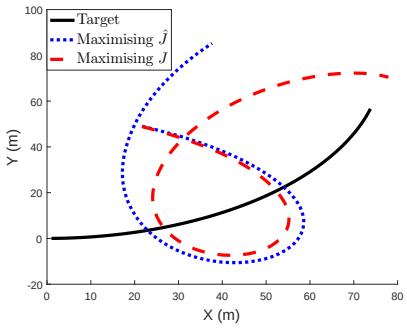

(c) Robot and target trajectories of case 3

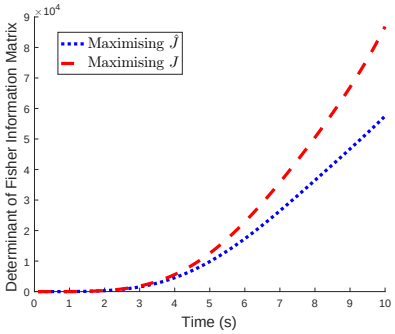

(d) Determinant of FIM of case 1

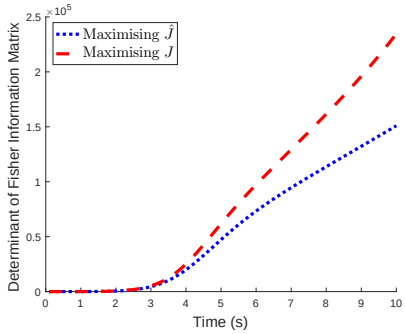

(e) Determinant of FIM of case 2

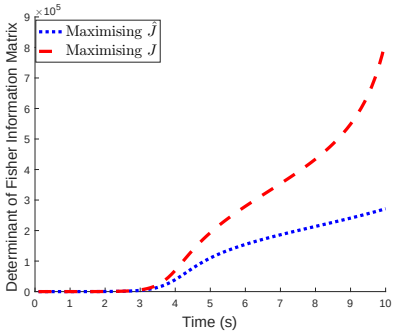

(f) Determinant of FIM of case 3

Fig. 9. Simulation results obtained from the proposed algorithm and [14] for three different target motions. The first column corresponds to stationary target; the second column refers to non-manoeuvring target; and the third column is for constant-manoeuvring target.

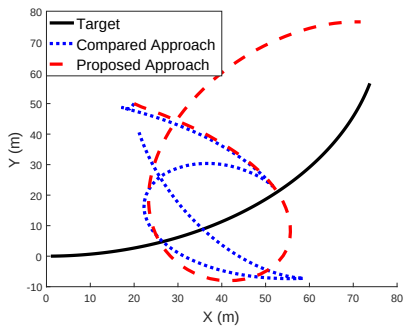

(a) Robot and target trajectories

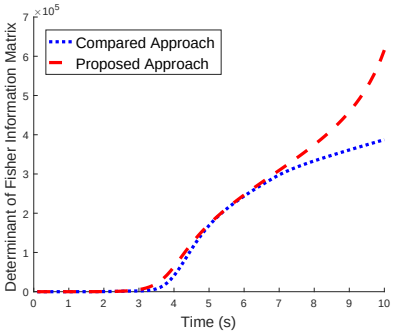

(b) Determinant of FIM

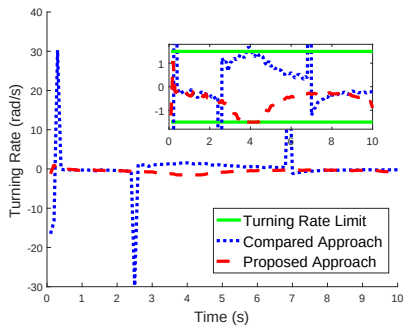

(c) Robot turning rate

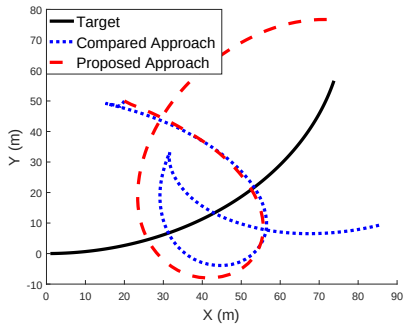

(d) Robot and target trajectories

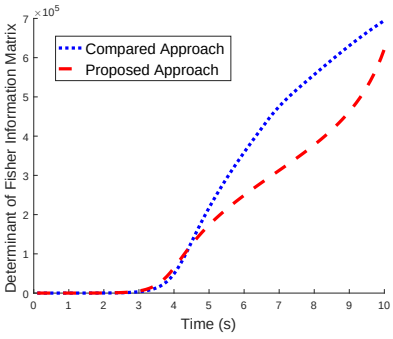

(e) Determinant of FIM

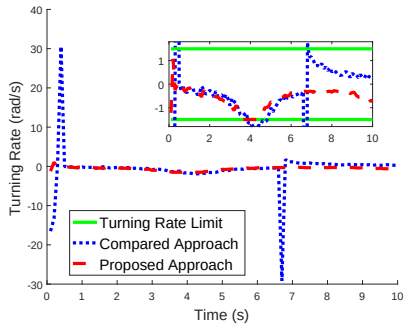

(f) Robot turning rate

Fig. 10. Simulation results obtained from the proposed algorithm and [42] for constant-manoeuvring target with each row corresponding to one sample run. The difference between these two rows is resulted from the multiple solution problem of [42].

TABLE II
RMSE COMPARISONS OVER1000 MONTE-CARLO RUNS.

	Metric	Case 1	Case 2	Case 3
Compared approach [42]	Mean	$1.5031m$	$1.5472m$	$2.1336m$
	Std	$0.7319m$	$0.8011m$	$1.0338m$
Proposed approach	Mean	$1.5027m$	$1.5408m$	$2.0562m$
	Std	$0.4059m$	$0.5466m$	$0.6412m$

considering the physical turning rate constraint, the proposed algorithm only generates one unique feasible optimal solution. When the candidate optimal heading angles generated by Theorem 1 locate outside the maximum permissible movement region, the final optimal solution is obtained by using the maximum turning rate, as shown in Theorem 2. This fact can be clearly observed from the zoomed-in figure in the third column of Fig. 10. Also, it follows from the second column of Fig. 10 that the determinant of FIM depends on robot's trajectory and one-step minimisation of the trace of the error covariance does not always ensure higher value of $|F|$ than maximising the proposed geometric cost function J.

To further evaluate the performance of these two different algorithms under various conditions, Monte-Carlo simulations with same random initialisations, shown in previous subsection, are conducted. The time average and standard deviation (Std) of RMSE for cases 1-3 over 1000 Monte-Carlo runs are summarised in Table II. Similar to previous subsection, t-test is performed with 5% significance level to check the statistical difference and the result is $h = 0$ for all three cases. It was shown in [1] that the trace of error covariance matrix or the inverse of FIM, known as A-optimality criterion, captures the geometric system dependencies. Therefore, it is expected that maximising the proposed cost function or minimising the trace of error covariance will generate comparable performance under same conditions. This can be clearly observed from Table II and confirmed by the t-test results. However, it is clear from Table II that the standard deviation of RMSE generated by algorithm [42] is larger than the proposed algorithm. The reason is that algorithm [42] might provide multiple solutions and will numerically pick up one solution from the solution set, which means that algorithm [42] might generate totally different trajectories with the same initial conditions, as we can note from the first column of Fig. 10. As a comparison, the proposed algorithm generates a unique and consistent solution with the consideration of physical constraints. Therefore, the advantage of the proposed approach, compared to [42] is clear: the algorithm developed considers the turning rate limit in trajectory optimisation. Therefore, the proposed algorithm is more practical and promising for real applications.

VI. CONCLUSIONS

The problem of analytical trajectory optimisation for target localisation with bearing-only measurement is studied in this paper. System observability is analysed in the relative domain by using geometric conditions. This provides better understanding of how observability influences the estimation performance. By leveraging the geometric performance measure derived as the cost function, the optimal observer heading command is derived analytically and the maximum permissible turning rate is also considered in the proposed approach. Extensive numerical simulations with comparisons are performed to validate the analytical finds.

REFERENCES

[1] S. Ponda, R. Kolacinski, and E. Frazzoli, "Trajectory optimization for target localization using small unmanned aerial vehicles," in *AIAA Guidance, Navigation, and Control Conference*, 2009.

[2] H. Roh, M.-H. Cho, and M.-J. Tahk, "Trajectory optimization using cramér-rao lower bound for bearings-only target tracking," in *AIAA Guidance, Navigation, and Control Conference*, 2018.

[3] A. M. Fosbury and J. L. Crassidis, "Optimal trajectory determination for increased relative navigation observability of air vehicles," in *AIAA Guidance, Navigation, and Control Conference*, 2008.

[4] A. I. Mourikis and S. I. Roumeliotis, "Optimal sensor scheduling for resource-constrained localization of mobile robot formations," *IEEE Transactions on Robotics*, vol. 22, no. 5, pp. 917–931, 2006.

[5] A. Ahmad, G. Lawless, and P. Lima, "An online scalable approach to unified multirobot cooperative localization and object tracking," *IEEE Transactions on Robotics*, vol. 33, no. 5, pp. 1184–1199, 2017.

[6] F. Morbidi and G. L. Mariottini, "Active target tracking and cooperative localization for teams of aerial vehicles," *IEEE Transactions on Control Systems Technology*, vol. 21, no. 5, pp. 1694–1707, 2013.

[7] S. C. Nardone and V. J. Aidala, "Observability criteria for bearings-only target motion analysis," *IEEE Transactions on Aerospace and Electronic systems*, no. 2, pp. 162–166, 1981.

[8] S. E. Hammel and V. J. Aidala, "Observability requirements for three-dimensional tracking via angle measurements," *IEEE Transactions on Aerospace and Electronic Systems*, no. 2, pp. 200–207, 1985.

[9] M.-J. Tahk, H. Ryu, and E.-J. Song, "Observability characteristics of angle-only measurement under proportional navigation," in *SICE'95. Proceedings of the 34th SICE Annual Conference. International Session Papers*. IEEE, 1995, pp. 1509–1514.

[10] E. Fogel and M. Gavish, "Nth-order dynamics target observability from angle measurements," *IEEE Transactions on Aerospace and Electronic Systems*, vol. 24, no. 3, pp. 305–308, 1988.

[11] D. C. Woffinden and D. K. Geller, "Observability criteria for angles-only navigation," *IEEE Transactions on Aerospace and Electronic Systems*, vol. 45, no. 3, pp. 1194–1208, 2009.

[12] J. Grzymisch and W. Fichter, "Observability criteria and unobservable maneuvers for in-orbit bearings-only navigation," *Journal of Guidance, Control, and Dynamics*, vol. 37, no. 4, pp. 1250–1259, 2014.

[13] T. L. Song, "Observability of target tracking with bearings-only measurements," *IEEE Transactions on Aerospace and Electronic Systems*, vol. 32, no. 4, pp. 1468–1472, 1996.

[14] P. Anjaly and A. Ratnoo, "Observability enhancement of maneuvering target with bearings-only information," *Journal of Guidance, Control, and Dynamics*, vol. 41, no. 1, pp. 184–198, 2018.

[15] S. Hammel, P. Liu, E. Hilliard, and K. Gong, "Optimal observer motion for localization with bearing measurements," *Computers & Mathematics with Applications*, vol. 18, no. 1-3, pp. 171–180, 1989.

[16] W. Lee, H. Bang, and H. Leeghim, "Cooperative localization between small uavs using a combination of heterogeneous sensors," *Aerospace Science and Technology*, vol. 27, no. 1, pp. 105–111, 2013.

[17] A. N. Bishop, B. Fidan, B. D. Anderson, K. Doğançay, and P. N. Pathirana, "Optimality analysis of sensor-target localization geometries," *Automatica*, vol. 46, no. 3, pp. 479–492, 2010.

[18] S. Xu and K. Doğançay, "Optimal sensor placement for 3-d angle-of-arrival target localization," *IEEE Transactions on Aerospace and Electronic Systems*, vol. 53, no. 3, pp. 1196–1211, 2017.

[19] K. Zhou and S. I. Roumeliotis, "Optimal motion strategies for range-only constrained multisensor target tracking," *IEEE Transactions on Robotics*, vol. 24, no. 5, pp. 1168–1185, 2008.

[20] J. L. Speyer, D. G. Hull, S. Larson, and C. Tseng, "Estimation enhancement by trajectory modulation for homing missiles," *Journal of Guidance, Control, and Dynamics*, vol. 7, no. 2, pp. 167–174, 1984.

[21] Y. Oshman and P. Davidson, "Optimization of observer trajectories for bearings-only target localization," *IEEE Transactions on Aerospace and Electronic Systems*, vol. 35, no. 3, pp. 892–902, 1999.

[22] T. L. Song and T. Y. Um, "Practical guidance for homing missiles with bearings-only measurements," *IEEE Transactions on Aerospace and Electronic Systems*, vol. 32, no. 1, pp. 434–443, 1996.

[23] P. Liu, "An optimum approach in target tracking with bearing measurements," *Journal of Optimization theory and Applications*, vol. 56, no. 2, pp. 205–214, 1988.

[24] R. Bajcsy, Y. Aloimonos, and J. K. Tsotsos, "Revisiting active perception," *Autonomous Robots*, vol. 42, no. 2, pp. 177–196, 2018.

[25] J. Le Cadre, "Optimization of the observer motion for bearings-only target motion analysis," in *Decision and Control, 1997., Proceedings of the 36th IEEE Conference on*, vol. 4. IEEE, 1997, pp. 3126–3131.

[26] J.-M. Passerieux and D. Van Cappel, "Optimal observer maneuver for bearings-only tracking," *IEEE Transactions on Aerospace and Electronic Systems*, vol. 34, no. 3, pp. 777–788, 1998.

[27] P. Tokekar, J. Vander Hook, and V. Isler, "Active target localization for bearing based robotic telemetry," in *Intelligent Robots and Systems (IROS), 2011 IEEE/RSJ International Conference on*. IEEE, 2011, pp. 488–493.

[28] J. Taylor, "The cramer-rao estimation error lower bound computation for deterministic nonlinear systems," *IEEE Transactions on Automatic Control*, vol. 24, no. 2, pp. 343–344, 1979.

[29] H. Bayram, J. Vander Hook, and V. Isler, "Gathering bearing data for target localization," *IEEE Robotics and Automation Letters*, vol. 1, no. 1, pp. 369–374, 2016.

[30] A. Logothetis, A. Isaksson, and R. J. Evans, "An information theoretic approach to observer path design for bearings-only tracking," in *Decision and Control, 1997., Proceedings of the 36th IEEE Conference on*, vol. 4. IEEE, 1997, pp. 3132–3137.

[31] ——, "Comparison of suboptimal strategies for optimal own-ship maneuvers in bearings-only tracking," in *American Control Conference, 1998. Proceedings of the 1998*, vol. 6. IEEE, 1998, pp. 3334–3338.

[32] E. W. Frew, "Trajectory design for target motion estimation using monocular vision," Ph.D. dissertation, Ph. D. dissertation, Stanford University, Stanford, CA, 2003.

[33] F. Lorussi, A. Marigo, and A. Bicchi, "Optimal exploratory paths for a mobile rover," in *Robotics and Automation, 2001. Proceedings 2001 ICRA. IEEE International Conference on*, vol. 2. IEEE, 2001, pp. 2078–2083.

[34] P. Salaris, R. Spica, P. R. Giordano, and P. Rives, "Online optimal active sensing control," in *Robotics and Automation (ICRA), 2017 IEEE International Conference on*. IEEE, 2017, pp. 672–678.

[35] M. Cognetti, P. Salaris, and P. Robuffo, "Optimal active sensing with process and measurement noise," in *ICRA 2018-IEEE International Conference on Robotics and Automation*, 2018, pp. 1–8.

[36] J. Vander Hook, P. Tokekar, and V. Isler, "Cautious greedy strategy for bearing-based active localization: Experiments and theoretical analysis," in *Robotics and Automation (ICRA), 2012 IEEE International Conference on*. IEEE, 2012, pp. 1787–1792.

[37] ——, "Cautious greedy strategy for bearing-only active localization: Analysis and field experiments," *Journal of Field Robotics*, vol. 31, no. 2, pp. 296–318, 2014.

[38] S. Xu, K. Doğançay, and H. Hmam, "Distributed pseudolinear estimation and uav path optimization for 3d aoa target tracking," *Signal Processing*, vol. 133, pp. 64–78, 2017.

[39] J. Vander Hook, P. Tokekar, and V. Isler, "Algorithms for cooperative active localization of static targets with mobile bearing sensors under communication constraints," *IEEE Transactions on Robotics*, vol. 31, no. 4, pp. 864–876, 2015.

[40] D. C. Woffinden and D. K. Geller, "Optimal orbital rendezvous maneuvering for angles-only navigation," *Journal of Guidance, Control, and Dynamics*, vol. 32, no. 4, pp. 1382–1387, 2009.

[41] H. Yu, R. Sharma, R. W. Beard, and C. N. Taylor, "Observability-based local path planning and obstacle avoidance using bearing-only measurements," *Robotics and Autonomous Systems*, vol. 61, no. 12, pp. 1392–1405, 2013.

[42] K. Zhou and S. I. Roumeliotis, "Multirobot active target tracking with combinations of relative observations," *IEEE Transactions on Robotics*, vol. 27, no. 4, pp. 678–695, 2011.

[43] K. Dogancay, "Uav path planning for passive emitter localization," *IEEE Transactions on Aerospace and Electronic systems*, vol. 48, no. 2, pp. 1150–1166, 2012.

[44] P. Tichavsky, C. H. Muravchik, and A. Nehorai, "Posterior cramér-rao bounds for discrete-time nonlinear filtering," *IEEE Transactions on Signal Processing*, vol. 46, no. 5, pp. 1386–1396, 1998.

Shaoming He was born in 1991. He received his MSc degree in Aerospace Engineering from Beijing Institute of Technology in 2016. He is currently a PhD student in the School of Aerospace, Transport and Manufacturing, Cranfield University. His research interests include multi-target tracking, guidance and control.

Hyo-Sang Shin received his BSc from Pusan National University in 2004 and gained an MSc on flight dynamics, guidance and control in Aerospace Engineering from KAIST and a PhD on cooperative missile guidance from Cranfield University in 2006 and 2010, respectively. He is currently Reader on Guidance, Control and Navigation Systems in Autonomous and Intelligent Systems Group at Cranfield University. His current research interests include multiple target tracking, probabilistic target detection and distributed control of multiple agent systems.

Antonios Tsourdos obtained a MEng in electronic, control and systems engineering from the University of Sheffield (1995), an MSc in systems engineering from Cardiff University (1996), and a PhD in nonlinear robust missile autopilot design and analysis from Cranfield University (1999). He is a Professor of Control Engineering with Cranfield University, and was appointed Head of the Centre for Cyber-Physical Systems in 2013. He was a member of the Team Stellar, the winning team for the UK MoD Grand Challenge (2008) and the IET Innovation Award (Category Team, 2009).

Trajectory optimization for target localisation with bearing-only measurement

He, Shaoming

2019-02-27

Shaoming He, Hyo-Sang Shin and Antonios Tsourdos. Trajectory optimization for target localisation with bearing-only measurement. IEEE Transactions on Robotics, Volume 35, Issue 3, 2019, pp. 653-668

https://doi.org/10.1109/TRO.2019.2896436